TAMPEREEN TEKNILLINEN YLIOPISTO
TAMPERE UNIVERSITY OF TECHNOLOGY

SHADI MAHDIANI

AN AUTOMATED APPROACH: FROM PHYSIOLOGICAL SIGNALS CLASSIFICATION TO SIGNAL PROCESSING AND ANALYSIS

Master of Science thesis

Examiner: Prof. Jari Viik
Examiner and topic approved by the
Faculty Council of the Faculty of
Natural Sciences
on 6th April 2016

ABSTRACT

SHADI MAHDIANI: An automated approach: from physiological signals classification to signal processing and analysis
Tampere University of Technology
Master of Science thesis, 77 pages
28 December 2016
Master's Degree Programme in Electrical Engineering Technology
Major: Medical Instrumentation
Examiner: Prof. Jari Viik
Keywords: signal processing, classifier, QRS detection, PVC detection, physiological signals

By increased and widespread usage of wearable monitoring devices a huge volume of data is generated which requires various automated methods for analyzing and processing them and also extracting useful information from them. Since it is almost impossible for physicians and nurses to monitor physical activities of their patients for a long time, there is a need for automated data analysis techniques that abstract the information and highlight the significant events for clinicians and healthcare experts.

The main objective of this thesis work was towards an automatic digital signal processing approach from physiological signal classification to processing and analyzing the two most vital physiological signals in long-term healthcare monitoring (ECG and IP). At the first stage, an automated generic physiological signal classifier for detecting an unknown recorded signal was introduced and then different algorithms for processing and analyzing the ECG and IP signals were developed and evaluated. This master thesis was a part of DISSE project which its aim was to design a new health-care system with the aim of providing medical expertise more accessible, affordable, and convenient. In this work, different publicly available databases such as MIT-BIH arrhythmia and CEBS were used in the development and evaluation phases.

The proposed novel generic physiological signal classifier has the ability to distinguish five types of physiological signals (ECG, Resp, SCG, EMG and PPG) from each other with 100 % accuracy. Although the proposed classifier was not very successful in distinguishing lead I and II of ECG signal from each other (error of 27%

was reported) which means that the general purpose features were enough discriminating to recognize different physiological signals from each other but not enough for classifying different ECG leads.

For ECG processing and analysis section, three QRS detection methods were implemented which modified Pan-Tompkins gave the best performance with 97% sensitivity and $96,45\%$ precision. The morphological based ectopic detection method resulted in sensitivity of $85,74\%$ and specificity of $84,34\%$. Furthermore, for the first PVC detection algorithm (sum of trough) the optimal threshold and range were studied according to the AUC of ROC plot which the highest sensitivity and specificity were obtained with threshold of -5 and range of $11:25$ that were equal to 87% and 82%, respectively. For the second PVC detection method (R-peak with minimum) the best performance was achieved with threshold of -0.7 that resulted in sensitivity of 68% and specificity of 72%. In the IP analysis section, an ACF approach was implemented for respiratory rate estimation. The estimated respiration rate obtained from IP signal and oronasal mask were compared and the total MAE and RMSE errors were computed that were equal to 0.40 cpm and 1.20 cpm, respectively. The implemented signal processing techniques and algorithms can be tested and improved with measured data from wearable devices for ambulatory applications.

PREFACE

This thesis work has been written for Department of Electronics and Communications Engineering at Tampere University of Technology and that was supported by the Finnish Funding Agency for Technology and Innovation (TEKES) as a part of Disappearing Sensors (DISSE) project (decision ID 570/31/2015) which was cooperated with GE Healthcare, Clothing+, and Elisa. The main objective of this master thesis was to develop and utilize different signal processing algorithms for processing and analyzing the two most vital physiological signals in healthcare monitoring applications: electrocardiography (ECG) and electrical impedance pneumography (IP).

I wish to express my gratitude to my supervisor Prof. Jari Viik for giving me this opportunity to be a part of this very interesting project and all his guidance and patience during the time it took to finalize this master of science thesis. I would like also thank all the member of DISSE project for providing an inspiring and communicative working environment.

I would like to thank Vala Jeyhani for his support during this work. Finally, I am grateful to my family and friends who have been there for me whenever their support and help was needed during this year.

Tampere, 01.09.2016

Shadi Mahdiani

TABLE OF CONTENTS

LIST OF FIGURES

LIST OF TABLES

LIST OF ABBREVIATIONS AND SYMBOLS

4G	Fourth Generation
ACF	Autocorrelation function
ADC	analog to digital converter
ANS	autonomic nervous system
AR	Autoregressive
AUC	area under the curves
AV node	Atrioventricular node
bpm	beat per minute
CEBS	Combined measurement of ECG, breathing and seismocardiogram
CMRR	common mode rejection ratio
cpm	cycle per minute
DISSE	Dissapearing Sensors
DSP	digital signal processing
E_s	Energy
ECG	electrocardiography
FFT	Fast Fourier Transform
FIR	finite impulse response
FN	false negative
FP	false positive
HR	Heart Rate
HRV	Heart rate variability
IoT	Internet of Things
IP	impedance pneumography
LED	light-emitting diode
M-Health	mobile health
MA	Moving Average
MAE	mean absolute error
MDF	Median Frequency
MNF	Mean Frequency
NB	normal beat
NN	Neural Networks
PAC	premature atrial contractions
PE	percent error

PFB	Population Reference Bureau
PPG	photoplethysmography
PVC	premature ventricular contractions
Resp	respiratory signal
RMSE	root mean square error
ROC	receiver operating characteristic
RRI	RR interval
SA node	Sinoatrial Node
SEN	Spectral Entropy
ShEN	Shannon Entropy
SNR	signal to noise ratio
TN	true negative
TP	true positive
TUT	Tampere University of Technology
WBSN	wireless body sensor network
WCT	Wilson central terminal
WGN	white Gaussian noise
WHMS	wearable health-monitoring systems
ZCR	Zero Crossing Rate

1. INTRODUCTION

Wireless sensor technologies with various applications in different fields of science and industry such as healthcare, transportation, travel, emergency systems etc. have potential to change our lifestyle in a way to overcome our everyday challenges. In recent years one of the main issues in developed countries is increasing population of elderly. Based on Population Reference Bureau (PFB) by 2050 people aged 65 or older will become twenty percent of total population [6]. Therefore, number of patients suffering from age related disease such as cardiovascular complications, Alzheimer, atherosclerosis, type 2 diabetes and hypertension will be increasing more and more [7]. Hence there is a need for providing healthcare systems and services for this rapidly growing population. Tele-monitoring systems by using wearable sensors are able to answer this need by monitoring people during their daily activities in-home and out of hospitals. With this solution, continuous non-invasive or invasive health monitoring cares and services can be provided with the minimum interaction between caregivers and patients.

Wearable physiological monitoring technology has quickly become a mainstream in long-term monitoring applications. During recent years, number of the wearable devices that monitor the health status of their users has been magnificently increased and we have witnessed a large popularity among both young and old generations. In addition, in professional sports, many athletes and teams are using smart clothes and equipment with embedded sensors that track and record their both physical and physiological data such as heart rate, speed, workload, distance and etc. [8]. Figure 1.1 illustrates an example of different wireless and wearable devices in different sections of our lives and their potentials to revolutionize prevention of disease, health monitoring and treatment process, self-health awareness, entertainment and business tools.

There are thousands of healthcare wearable devices and gadets that could help people to live healthier and better. Smart watches, wristband activity trackers,

Figure 1.1 *Wireless and wearable gadgets entry's into different sections of our lives such as fun and entertainment, healthcare, business and sports that influences our lifestyles in many ways and improves the quality of our lives [image purchased from Dreamstime.com]*

smart glasses, wearable cameras, smart clothes and motion sensing shoes are just a few examples of these technologies. According to the latest analyst report in 2014, Goode Intelligence has forecasted that there will be more that 5.5 billion users of mobile and wearable biometric technology around the globe by 2019.

By increased widespread usage of healthcare wearable monitoring devices a huge volume of data is created everyday. Clearly, it is an impossible task for medical experts to analyze and check this amount of data, hence, there is a need for automated analysis tools and techniques that can extract significant information for them. This kind of information then can be used in diagnosis ans treatment purposes.

This master thesis is a part of Disappearing Sensors (DISSE) project which focuses on new services and care processes that will be enabled by wearable long-term measurements systems and an Internet of Things (IoT) platform. This new approach will become available for both hospitals and home care purposes. In DISSE project, the physiological data is captured by a measurement circuit, sent through a wireless

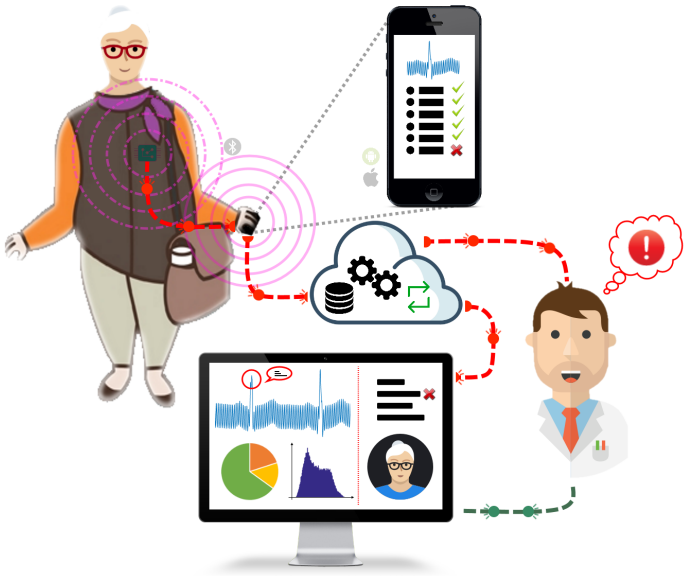

Figure 1.2 *Architechture of DISSE project, that includes active measurements circuit (electrodes are integrated to clothes) , wireless communication (Bluetooth, mobile device and WiFi), data storage and analysis (performed on an IoT cloud platform) and graphical user interfaces (designed in two version of patients and medical experts) sections*

communication channel, stored on a cloud platform in which it is also analyzed by automatic algorithms and eventually the outcome is presented to the user through a graphical user interface (GUI). Figure 1.2 shows whole architecture of DISSE project from patient side to the medical experts interface.

In DISSE project, two most vital physiological signals in healthcare monitoring: electrocardiography (ECG) and impedance pneumography (IP) that have the major impact on health condition of people especially elderly are measured and proper methods and algorithms for processing and analyzing them are investigated. In this project, active electrodes are integrated to the clothes for user comfort and wash ability need. Since then the measured data are transferred through Bluetooth to a mobile device and then through Wi-Fi to the cloud service. At this point, various signal processing methods are needed for processing and analyzing these long-term measured data and extracting important parameters from them; which is the topic of this master thesis. These parameters and biomarkers can be useful for clinicians and healthcare experts in their diagnosis and treatment processes.

In this regard, design and development of wearable and well-being devices has attracted lots of attention in industry and scientific associations in the last decade. Advanced and miniaturized electronics with signal acquisition technologies provide a possibility for designing only one device with several physiological measurement purposes. In this thesis work, we also proposed an automated generic physiological signals classifier for detecting unknown recorded signals. Our motivation for this classifier was toward an automatic healthcare monitoring system that the user can easily attach the electrodes to the body and the device automatically detects the measured signal and changes its settings to the appropriate mode for analysis and representation parts. The generic classifier could be implemented in medical monitoring devices for the purpose of merging multiple wearable devices into one piece and simplifying the usage of them for long-term purposes. In the following, different data processing methods and analysis techniques depending on the measured physiological signals (ECG and IP) are discussed and implemented.

In Chapter 2, the background for this thesis work is covered; by taking a look at history of wearable technologies in healthcare application, the importance of physiological signals such as ECG and IP, reviewing data processing and analysis methods used in the literature for applications involving wearable sensing technologies. In Chapter 3, steps of the proposed classifier are described in details and different methods and algorithms for analysis of ECG and IP signals are discussed. At the end, results of the generic classifier and signal processing algorithms are presented in 4. And the last chapter 5 is dedicated to conclusion of this thesis work.

2. THEORETICAL BACKGROUND

2.1 Wearable Technologies in Healthcare Monitoring

In developed countries, fast growth in aging population, has accompanied an increase in the demand for healthcare services that resulted in high healthcare costs during last decade [9]. Hence, there has been a need for decreasing these costs and providing healthcare services available at anytime and anywhere. Monitoring health condition of this group of population at home and during their daily activities can be resulted in lower healthcare costs, less high risk health conditions and more self-awareness. On the other hand, the fast increase in availability, miniaturization and enhanced data rates of mobile communication systems like Fourth Generation (4G) of digital cellular networks, has had an impact on accelerating the deployment of mobile health (M-Health) systems and services in recent years. In other words, mobile communications and network technologies with the help of wearable electronics have merged to create wearable health monitoring systems [10].

Wearable health-monitoring systems (WHMS) have attracted lots of attention in research areas and industries during the recent years [11–13]. A big variety of commercial products and prototypes have been produced with the goal of providing real-time feedback to the user or to a medical center and professional physicians, while including an alert system in the case of possible imminent health threatening conditions.

Wearable medical systems may consist of various types of miniature sensors, wearable or even implantable ones. These biosensors can measure significant physiological data from body such as electrocardiogram, heart rate, respiration rate, blood pressure, body temperature, oxygen saturation, etc. The recorded parameters are transferred through Bluetooth and Wi-Fi to a server for storage and analysis. Generally, healthcare wearable devices contain various components like sensors, wearable materials, smart textiles, actuators, power supplies, wireless communication

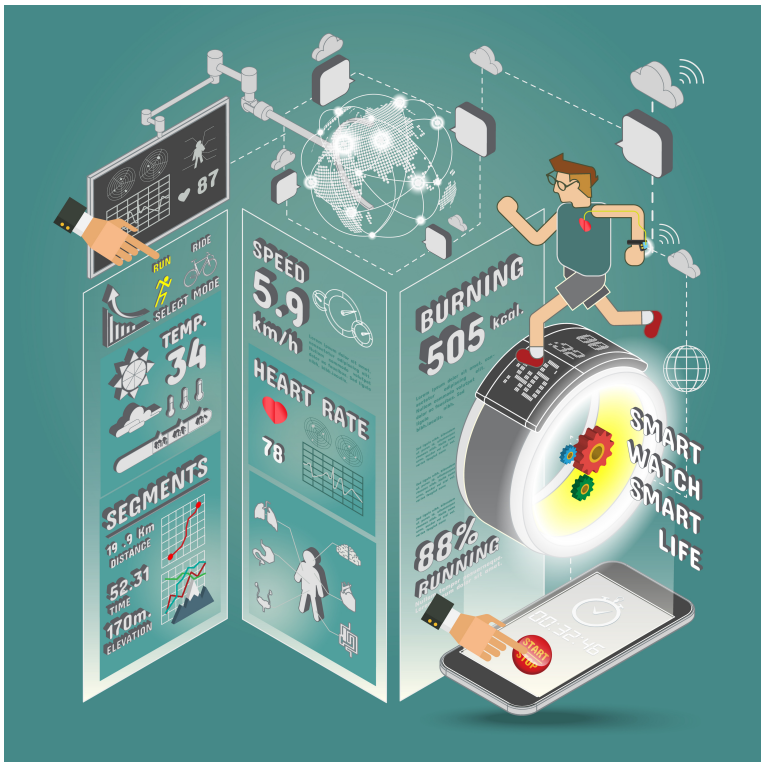

Figure 2.1 *An example of using wearable technologies such as smart watches and smart clothes during our daily activities; that provide useful information about our health and physical condition such as heart rate changes, speed of running/walking, heart activity during running/walking, number of steps during a day, burned calories and so on [image purchased from Dreamstime.com].*

modules, control and processing units, user interface, and decision making algorithms [14].

Fig. 2.1 illustrates a well-defined example of using wearable health monitoring and well-being devices that affect our life styles and meanwhile can improve the quality of our lives. In this picture 2.1, the user's heart activity is being monitored by the sensors integrated into his shirt and then the data is being transferred to his smart watch. In addition, his motion activities are also recorded by e.g. accelerometer sensors that can be embedded in the smart watch. Since then, all the recorded data are being transferred to the storage server. In the cloud server, different automatic analysis algorithms can be applied on the data and some informative figures and trends are presented about user's well-being condition such as heart rate changes, speed of running/walking phases and heart rate changes during these phases, calories usage during different activities and so on. At the end, it can be concluded

that WHMS has created a new meaning in self-health awareness and health tele monitoring applications.

Besides well-being, sports, rehabilitation, entertainment products, wearable electronics and technologies have also expanded possibilities to improve long-term monitoring applications in a totally new way. Long-term monitoring has been always a significance way for discovering abnormities in vital signs and avoiding life threatening situations. With the help of wearable electronics and technologies, long-term monitoring can be available with low cost at anytime and anywhere.

2.2 Advanced Intelligent Systems in Healthcare Applications

In the past decade, with the fast developments and advancement in sensors and wireless technologies, the focus of health monitoring systems has been also updated from mainly obtaining the data to developing intelligent systems that perform a variety of tasks to help people with their physical and mental challenges [15]. These intelligent systems include pattern recognition and decision making algorithms, which can be used in disease detection and prevention, and personal health awareness tasks. Advance intelligent devices are drawing a serious attention in market since continuous health monitoring is becoming an inseparable part of healthcare processes.

Automated intelligent systems are able to answer the needs of healthcare professionals in analyzing, categorizing, and representing long-term physiological signals. Furthermore, due to the large increase of interest in wearable devices for long-term measurements, data gathering, data analyzing and data mining of physiological signals are currently a big challenge in health monitoring systems [16]. Nowadays wearable monitoring systems are used not only by elderly, athletes or patients but also increasingly by healthy people. Multi-functional devices can have a significant role in simplifying the usage of these monitoring devices, since users will be able to use only one device for monitoring their physiological phenomena instead of multiple devices one for each measurement purpose.

Fortunately, advanced electronic designs and available signal acquisition technologies (e.g. analog-front-end solutions) provide such a possibility for designing one device with various physiological measurements applications. For designing such a system, it is required to implement a simple generic classifier, which is able to detect the measured data and then automatically changes to the detected mode for the

further analysis and processing tasks. In this thesis work, a novel robust approach to physiological signals classification is introduced.

2.3 Physiology of Heart

The heart is the vital organ of the circulatory system that keeps pumping blood throughout the whole body. The heart is located in the center of the thorax, behind the sternum. The main responsibility of the heart is circulating the blood in the veins and enables a sufficient oxygen supply for other organs of body. Figure 2.2 illustrates the details structure of the heart. The heart consists of four separate champers which upper chambers on each side is called atrium and their responsibility is receiving and collecting the blood coming to the heart and then delivering the blood to the lower chambers. The lower left and right chambers are called ventricles that are responsible for rhythmic contractions and sending the blood away through the circulation. The right ventricle pumps the deoxygenated blood to the lungs through pulmonary arteries. Meanwhile, the left ventricle pumps the oxygenated blood through aorta to the whole body. [17, 18]

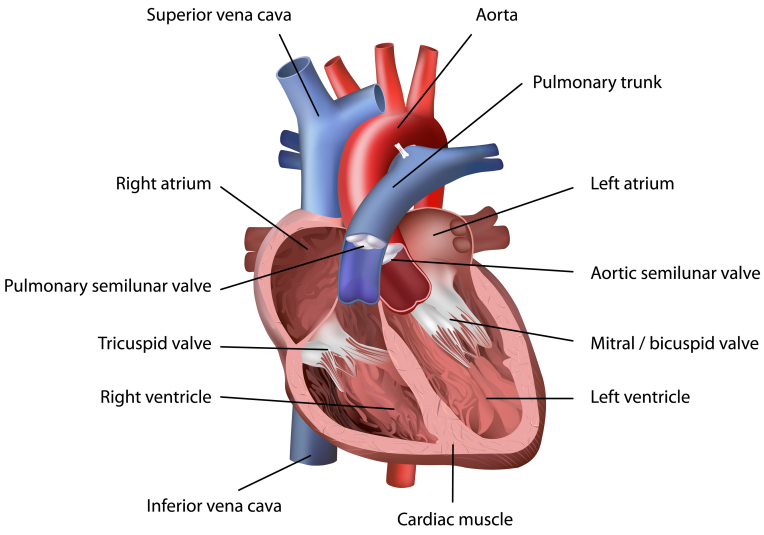

Figure 2.2 *Detailes structure of the heart, [image purchased from Dreamstime.com]*

Each pump of the heart includes two phases: systole and diastole. Systole phase is the time that cardiac muscle tissues in the ventricles are contracted while the atria are relaxed and filling. Diastole phase happens when cardiac muscle tissues in the

ventricles are relaxed and filling while atria contract. In this phase the ventricles make room for accepting the blood from atria. [19]

A network of nerve fibers controls the contraction and relaxation of cardiac muscle tissue for achieving the wave-like pumping action of the heart. The sinoatrial node (SA node) acts like an impulse generator for the heart and sends every electrical impulse of the heart. The SA node that is located in the area above of the right atrium, spreads the electrical activity through the atria and causes the muscle tissue contraction in a wave-like manner. After that the originated impulse from the SA node reaches the atrioventricular node (AV node) that is located in the lower area of the right atrium. The AV node also forwards an impulse via the nerve to the ventricles and initiates the same wave-like contraction in the ventricles. The electrical signal propagates from AV node through the right and left bundle branches and constructs the contraction of cardiac tissue muscle. [17–19]

In addition to the heart chambers, veins and arteries, the cardiovascular system also consists of the heart valves. These valves take care of direction of blood flow by preventing the backward flow in the circulatory system.

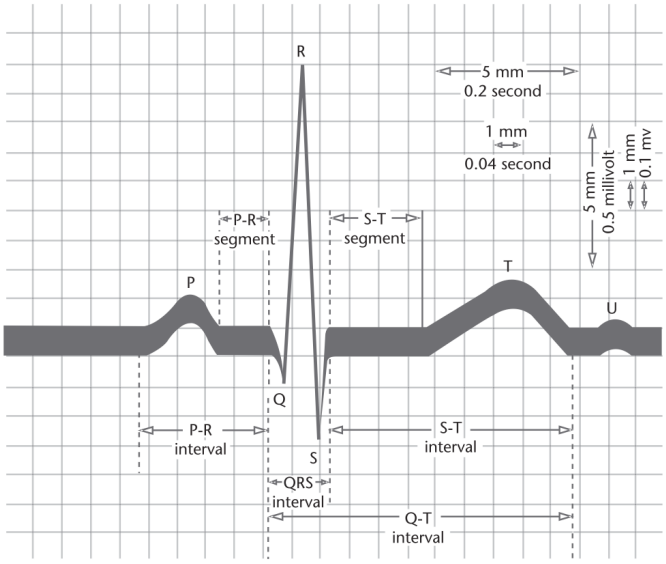

Figure 2.3 *Normal features of an ECG signals [1]*

2.4 Characteristics of ECG

Electrocardiography is a sequence of repolarization and depolarization states of atria and ventricles which produce P, QRS and T waves, and also with occasional U waves, that are connected with PR, ST and TP segments, respectively. The P wave represents right and left atrial depolarization, in consequence the PR interval is the time interval between onset of the P wave and onset of the QRS complex. The QRS complex itself represents ventricular depolarization. The ST segment (also called ST interval) is the time between ending point of the QRS complex and onset point of the T wave. And at the end, the T wave represents ventricular repolarization of the heart.

Figure 2.3 illustrates a normal clinical electrocardiography signal including the wave amplitudes and inter-wave timings. Some typical values of common clinical signatures of ECG signal along with their nominal range for a healthy adult are also presented in Table 2.1. Based on changes in the clinical signatures of heart in comparison to their nominal range, medical experts are able to assess heart diseases and malfunctions of heart. Although various parameters such as age, sex, food habits, gene etc. are usually taken into account for the actual clinical diagnosis.

Table 2.1 *Common ECG Signatures for clinical use [4]*

Clinical Signature	**Typical Values**	**Nominal limits**
P width	110 ms	± 20 ms
T width	180 ms	± 40 ms
PR interval	120 ms	± 20 ms
QRS width	100 ms	± 20 ms
QT_c interval	400 ms	± 40 ms
P Amplitude	0.15 mV	± 0.05 mV
T Amplitude	0.3 mV	± 0.2 mV
QRS Amplitude	1.2 mV	± 0.5 mV

2.5 ECG Measurement System

The electrical activity of the heart can be recorded from electrodes on the body surface. The standard 12-lead electrocardiogram is a standard representation of the

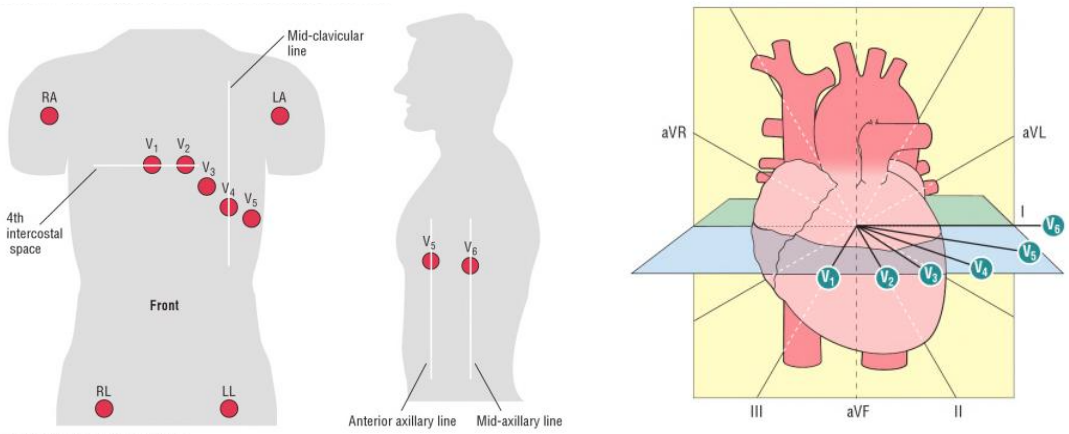

(a) Electrode placement (b) Leads in three dimensions

Figure 2.4 *Standard 12-lead ECG placement [2]*

heart's electrical activity which gives 12 different views of the heart. These views are recorded by placing three electrodes on the limbs (two arms and left leg), six electrodes on the patient's chest and one electrode on the right leg. The location of the chest electrodes are depicted in Figure 2.4(a).

The lead is a difference between every two potentials on the body. There are two types of leads: bipolar and unipolar. The limb leads I, II and III are bipolar and the three augmented limb leads (aVR, aVL, and aVF) and the six chest leads (V1, V2, V3, V4, V5, and V6) are unipolar (see Figure 2.4(a)). The bipolar leads are measured between two electrodes and unipolar leads, on the other hand, are measured with respect to a common point called Wilson central terminal (WCT). The six limb leads provide information about heart's frontal plane and the six chest leads that are placed in sequence across the chest, provide information about heart's horizontal plane (shown in Figure 2.4(b)). These six frontal plane leads (I, II, III) and six horizontal plane leads form the standard 12-lead ECG system which is the most common and accepted method for measuring ECG signal from a patient. [17]

Although 12-lead ECG measurement is the clinical standard, it is not required for well-being, wearable and tele monitoring applications. Wearable monitoring devices usually consist of one or few ECG leads as long as these leads have a good view of the different ECG waveforms. The main aim of ECG wearable systems is monitoring the patients with mild heart diseases continuously while they have their active lifestyle at the same time. Due to this reason, advanced miniaturization in electrical

components and circuits, ECG recorders have been getting available in very small size and low weight with capability of recording contentiously for long-term with a small battery. Fortunately, with the help of advanced stretchable electronic materials, printed active electrodes are also integrated to clothes and provide a wearable solution for ECG monitoring clothing [20]. Figure 2.5 demonstrates one example of wearable ECG monitoring system in a form of smart T-shirt that includes textile electronics and a Suunto wireless transmitter which transfers the data collected by garment sensors to a smartphone app.

Figure 2.5 *An example of wearable ECG monitoring system, integration of Clothing+ textile-integrated electronics (disappeared into fabrics for optimum comfort, durability and convenience) and Suunto wireless transmitter that transfers the recorded data to a smartphone app*

Artefacts in ECG

In wearable monitoring devices, the presence of noises and artefacts is inevitable. The ECG signal is usually disturbed with different types of artifacts. The nature and origin of these artifacts are exclusively important for long term monitoring applications. Practically, there are two types of artifacts which are caused due to physiological and non-physiological reasons [4, 21, 22]. Electromyography (EMG) noise and slow baseline wandering due to respiration are in category of physiological origin noises and power-line interference and motion artifacts are in category of non-physiological noises in ECG. The presence of the artifacts make any morphology based diagnosis problematic. The common sources of artefact that corrupt ECG signals are described in the following.

EMG Noise

Electromyography noise is produced during ECG monitoring due to any muscular activity in the body. Bandwidth of a surface EMG signal is in the range from 5 to 500 Hz which has overlap with spectrum of the ECG signal. Thus, any muscular activity may cause interference in the ECG signal. Generally, for clinical purposes the patient is usually in rest condition but in ambulatory or wearable applications and for long-term monitoring purposes, the presence of high frequency EMG noise is inevitable and the level of muscle noise depends quite significantly on the level of the patient activity [21].

Baseline Wandering

The baseline of ECG known as isoelectric line is a line recorded in the TP interval during the heart rhythms. Ideally the isoelectric line is considered to have zero amplitude and anything above the isoelectric line is considered positive and below the line is negative. Therefore, the baseline of the ECG signal should be at a constant level. Baseline wandering in ECG might happen due to respiration which alter the impedance path between the ECG electrodes and then results in a slowly varying potential difference. During long-term monitoring, baseline wandering is quite common and can easily be eliminated by applying a high pass filter on the recorded signals with cut-off frequency of e.g. 0.2 Hz. However, the low frequency components of ECG like P and T waves might be little disturbed because of this filtering [21].

Power-line Interference

Power-line interference is a common disturbance in bio-potential measurements which usually happens due to long wires between subject and amplifier, separation between electrodes, and capacitive coupling between subject and power-lines. Since the frequency of power-line is 50/60 Hz, it can be easily distinguished from the recorded signal by looking at the spectrum of the measured signal. If the distance between two leads of ECG is very small, the power-line currents would be the same in both leads and this power-line interference can be rejected with an instrumentation amplifier that has a very high common mode rejection ratio (CMRR) [1]. A

convenient way for eliminating this form of noise is using a single or multiple notch filter with notch frequency at 50/60 Hz and their harmonics.

Motion Artefacts

Motion artefact is produced by movements of electrodes and cause a non-steady baseline. Usually, for clinical purposes, the subject is in rest condition and hence the motion artefacts are inconsiderable but in long term wearable applications due to any type of motions, the impedance between skin and electrode interface might be disturbed and produce motion artefacts. Since ECG signal and produced motion artefacts have an overlap frequency range in their spectra, it is not easy to remove such an artefact from the recorded signal. Although the motion artefact poses a major challenge in wearable ECG monitoring, but usually can be partially eliminated by applying a high pass filter on the corrupted signal. [1, 21].

2.6 Arrhythmia, Ectopic Beats

Any abnormal cardiac rhythm is called arrhythmia. Atrial arrhythmias are the most common type of arrhythmias that occurs due to impulses originating from the area outside of the SA node. The origination of ventricular arrhythmias is from inside of the ventricles below the bundle of His. Ventricular arrhythmias happen when the electrical impulses that have the role of depolarizing the myocardium use a different pathway than the normal one. In ventricular arrhythmias, the QRS complex is usually wider than normal range due to the exceeding conduction time. The QRS complex and T wave may also appear in opposite directions due to the changes in action potential. In addition, when the atrial depolarization does not occur, the P wave may also be absent.

Ectopic beat is an irregular cardiac rhythm which mostly happens when heartbeat has its origin from fibers or group of fibers outside the region of the heart muscle rather than from the SA node. These irregular heart rhythms may lead to extra or skipped heartbeats. Usually the cause of ectopic beats is not clear and most people may experience extra or skipped beats on occasion. These beats are usually harmless and there is no need for medical treatment. The two most common types of ectopic heartbeats are: premature atrial contractions (PAC) (see Figure 2.6) and premature ventricular contractions (PVC) (see Figure 2.7). When the origin of

ectopic beat comes from atria, it is called PAC and when it comes from ventricles, it is known as PVC [2, 3].

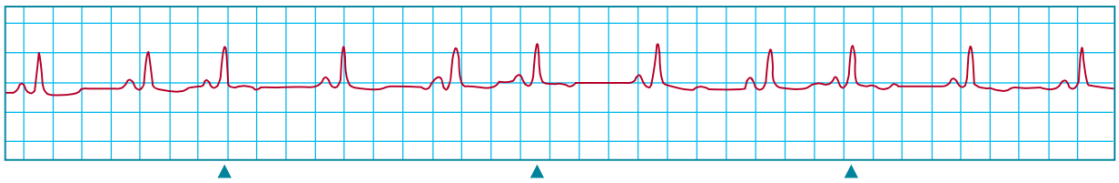

Figure 2.6 *Premature atrial contractions beats are marked with triangles below them. [3]*

PAC beats can be recognized based on the time interval between each two consecutive R peaks. It can be seen that the time interval between R peaks is narrower before PAC and wider after that. PVCs are more significant since the occurrences of them rise with age. PVCs can lead to more critical arrhythmias, like ventricular tachycardia or ventricular fibrillation. In addition, PVCs can be the cause of less cardiac output when they occur more often. The PVC beat is mostly wider, its reduced QRS complex happens early and the P wave is usually absent. The missing P wave cause distortion in the ST segment. In Figure 2.7 two typical types of PCVs are shown [2, 3].

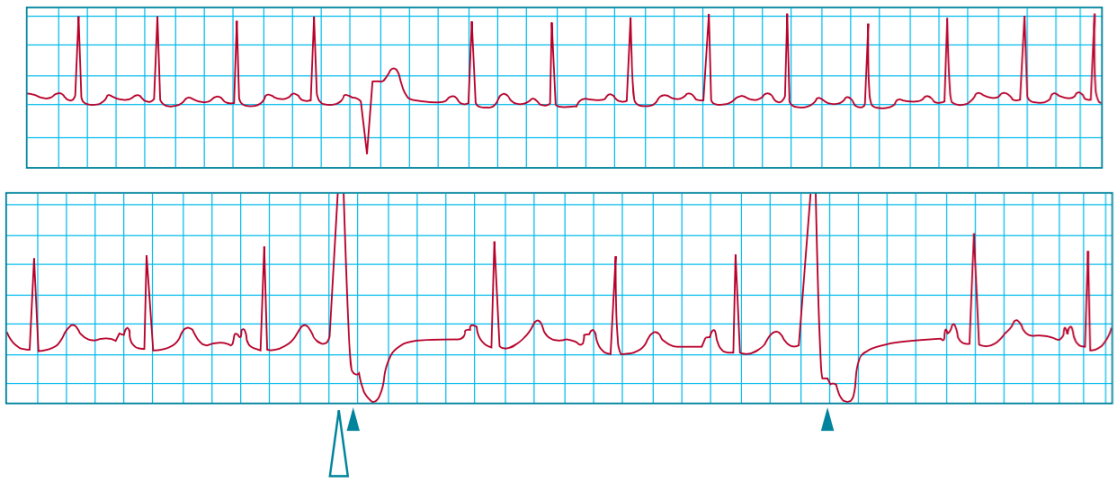

Figure 2.7 *Two typical types of premature ventricular contractions beats are shown. In top plot, the one abnormal beat corresponds to one type of PVC beats and, in below plot, the other typical type of PVC beats are marked with triangles below them. [3]*

2.7 Review of ECG Analysis Methods

By increased usage of wearable monitoring devices, everyday a huge volume of data is generated that raise the need for developing advanced analysis algorithms. ECG signal can be recorded by single-lead or multiple-lead depending on the configuration of the device and hence the automatic analysis methods differ based on the configuration. Single-lead ECG interpretation methods are mainly relying on the morphological parameters, repeatability of the heart cycle and their spectral features. In multi-lead ECG processing techniques the concurrency of features in different leads is also considered which result in more reliable outcomes in noisy environments. However, in wearable and ambulatory applications using multiple-lead for measurements are not applicable and cause discomfort and difficulty in daily usage for the patient. Therefore, single-lead algorithms are more used in wearable monitoring purposes and in this chapter some existing algorithms and methods for single-lead ECG signals are reviewed.

2.7.1 QRS Detection Methods

The QRS detection is the basis of every ECG processing and analysis algorithms. The R-peak is the most significant component in the QRS complex which can be distinguished by its high amplitude and sharp slopes. The heart rate is also computed by calculating the time interval between two consecutive R-peaks. Different arrhythmias can be detected based on the locations of R-peaks and some other ECG features. For instance, elevation or depression of ST segment is calculated based on the amplitude of the signal at a specific time interval from the end point of QRS complex [21, 23].

QRS detection methods have been attracted lots of attention during the last 20 years in research areas. Various approaches have been introduced for QRS detection such as artificial neural networks, machine learning tools, genetic algorithms, wavelets and filter banks and so on [24]. In the following, the basis of some of these algorithms are shortly described and their detection accuracy on a same database are compared.

Most of the QRS detection approaches are divided into two steps: pre-processing and decision making. Pre-processing step usually contains different filtering techniques for noise and artefact reduction such as low-pass, high-pass or band-pass filtering. Since the next step is usually based on thresholding, then the filtering stage is

necessary for reducing the impact of P and T waves amplitude that can lead to wrongly detected point as an R-peak. In most of the algorithms, after pre-processing, the QRS complex is detected in an adaptive or a non-adaptive thresholding process. The threshold level is mostly chosen in order to decrease wrongly detected points (false positives).

Arzeno et al. [25] introduced a simple derivate-based algorithm that uses a high-pass filter to determine the maximum slope, that corresponds to QRS complexes. In other algorithms more sophisticated filters are also used [26, 27]. Determining a threshold for maximum slope is set adaptively in [28, 29]. Generally, in neural network and machine learning based algorithms, some morphological characteristics and frequency components of QRS complexes from ECG databases are trained to a system and then the trained network is applied on an unseen ECG signal for detection of QRS complexes [30, 31].

In wavelet approaches, the ECG signal is decomposed to different frequency bands and then by applying a certain threshold according the QRS morphologies, the R-peaks are detected. Wavelet methods are more robust in noisy environments in comparison to the derivative methods which use simple filtering techniques [31]. Poli et al. [32] proposed an optimum QRS detectors. They performed the filtering phase by applying linear and non-linear polynomial filters to enhance the QRS complexes and then used an adaptive maximum detection approach for distinguishing QRS complexes from the rest of ECG signal. They have used a genetic algorithm for setting parameters of the filter and the detector in order to minimize the detection error.

Zhengzhong et al. [33] have presented a QRS complex detection technique for intelligent ECG monitoring. In pre-processing stage, firstly the power-line interference and baseline wander were removed. Afterwards, an improved Pan-Tompkins method was introduced for finding the location of R-peaks. Arteaga-Falconi et al. have presented a new QRS detection techniques based on the second derivative technique [34]. They introduced a peak detection method using a threshold that depends on the sampling frequency of the recorded signal. This method is useful for wearable application since it is computationally inexpensive that needs less power for detection of R-peaks. Table 2.2 shows the performance of each algorithm based on the result provided by their authors on MIT-BIH arrhythmia database [5].

Table 2.2 *Performance of the mentioned QRS detection algorithms on MIT-BIH arrhythmia database [5], provided by their authors*

Algorithm by	**Sensitivity %**	**Pos. Predictivity %**
Arzeno et al. [25]	99.68	99.63
Afonso et al. [27]	99.59	99.56
Pan & Tompkins [28]	99.30	-
Hamilton & Tompkins [29]	99.69	99.77
Xue et.al [30]	99.50	97.50
Abibullaev & Seo [31]	97.20	98.52
Poli et al. [32]	99.60	99.51
Zhengzhong et al. [33]	99.90	99.96
Arteaga-Falconi et al. [34]	99.43	99.22

2.7.2 PVC Detection Methods

One of the significant outcomes of long-term ECG monitoring is identification of abnormal heartbeats such as ventricular ectopic beats. Ventricular premature beat or PVC is a sign of disturbance in depolarization process of the heart that may lead to malignant cardiac arrhythmias [35]. Therefore, the detection of this arrhythmia becomes crucial in the early diagnosis which can prevent life threatening cardiac diseases in elderly patients. In the last decade, various fast automatic PVC detection methods have been developed. Some of these algorithms are briefly discussed in the following.

The classical PVC detection algorithms are based on extracting time domain features. Cho and Kwon [36] have used QRS width, RR interval (RRI), and QRS shape as time domain and morphological variables for distinguishing premature beats from normal ones. The QRS width was computed by defining the QRS starting and ending points which are Q and S point, respectively. Since the RR interval gets shorter before premature ventricular contraction and gets wider after that, the RR intervals were compared between normal and ectopic beats as a time domain variable. Eventually, the shape of normal QRS complexes in a template matching approach was used as the morphological feature in their work. They have evaluated their method on some records of MIT-BIH arrhythmia database and presented overall specificity and sensitivity of 99.30% and 98.66%, respectively

Basically, in time and morphological based algorithms, the QRS shape is the key factor for detecting the PVC beats from the normal ones. Supat et al. [37] developed a method with low computational cost for detecting premature ventricular contraction in real-time applications. The used features were QRS pattern and RR interval. They have implemented simple decision rules for classifying normal and premature beats and evaluated their technique on MIT-BIH Arrhythmia database. The obtained result was 91.05% sensitivity and 99.55% specificity. Although the proposed method has achieved a good performance but it is not robust to interferences in noisy environments. In conclusion, the advantage of time domain features based algorithms is low complexity which makes them suitable for implementing in real time monitoring systems. However, these methods are very sensitive in presence of noise and artefacts and may result in high number of false alarms.

Garcia and his colleagues [38], proposed a heartbeat detection and classification method by using four morphological characteristics and eight temporal features. The three morphological features were defined by calculating maximum cross-correlation between current, previous and following beats. The last morphological feature was related to QRS duration when the amplitude of R-peak is halved. The temporal features were basically related to RRIs. They applied discriminant analysis for classifying heart beats into three categories: PVC, PAC and normal beat (NB). They evaluated their algorithm with MIT-BIH Arrhythmia and MIT-BIH Supraventricular Arrhythmia databases and obtained sensitivities of 97.17%, 97.67% and 92.78% for correctly detected NB, PVC and PAC beats, respectively. They achieved very good performance in the detection of PVC and normal beats. This algorithm can be integrated in wearable measurement systems and analyze each recorded signal automatically beat to beat.

Chang and his colleagues [39] have presented a real time high precision PVC detection method. Initially, R-peak is detected by applying wavelet transform method and then two PVC detection algorithms, sum of trough and sum of R-peak with minimum are introduced for detecting every possible shapes of PVC beats. They evaluated their algorithms on four records of MIT-BIH Arrhythmia database which contained normal beats with PVCs only (No. 119), only normal beats (e.g. No. 100), different types and numbers of PVCs (No. 116) and mixed with other types of arrhythmia (No. 114) and eventually presented the average accuracy of 94.73%. In this master thesis, this PVC detection method was implemented and the obtained results are presented in the result chapter.

2.7.3 Heart Rate and Heart Rate Variability Analysis

Generally, studying the electrical activity of heart gives us lots of information about our body. Heart rate variability (HRV) has been known as a non-invasive tool for studying the operation of autonomic nervous system (ANS). HRV represents the variation between consecutive heartbeats and can be influenced by different physiological phenomena inside our body such as physical activity, exercise and recovery from physical activity, movements and changes in posture and also stressed and relaxed situations. HRV varies from day to day according to amount of work loads, physical activity and stress level.

Basically, heart rate and HRV follow an inverse relationship. In other words, heart rate variability is higher when the heart beats slowly and diminishes whenever the heart beats faster. HRV parameters are computed in time and frequency domain and represent activity of sympathetic and parasympathetic nervous system. Firstbeat Technologies Ltd. has developed various HRV based algorithms for stress and recovery analysis, metabolic processes and energy expenditure estimation, detection of movements and changes in posture. Firstbeat is the leading provider of physiological analytics for sports and well-being and their algorithms have been integrated into a variety of well-known wearable fitness and tracking products such as Samsung, Garmin and Suunto. Due to importance of HRV analysis, in this master thesis, different parameters of HRV are studied in the method chapter.

2.8 Respiratory Rate Monitoring

Respiratory rate is number of breaths per minute. Respiratory rate monitoring is one of the vital measurements for assessing the subject health condition in both clinical and well-being applications. There are various measuring methods for acquiring the respiratory rate. Spirometry is the golden standard method which measure the direct flow rate of breathing air. Spirometry is the most common pulmonary function test that provides the precise clinical information of long volume, speed of inhaled/exhaled air, respiratory rate etc. Other approaches such as thermography by using nasal or oronasal thermistor [40, 41], monitoring the pressure by using facemask [42] also employed for estimating the respiratory rate. However, none of above methods are applicable in wearable applications.

Other methods such as impedance pneumography [43], inductance pneumography

[44] and using physiological signals like electrocardiography and photoplethysmography (PPG) [45, 46] were developed for monitoring respiratory rate in ambulatory and wearable cases. In these methods, sensors are not required to be placed on the facial area, then it provides more comfortable situation for the patient. In addition, IP technique has another significant advantage in comparison to the other methods, that is the ability to be recorded from the ECG electrodes on the body surface and it does not require additional sensors or electrodes worn by the user. In DISSE project, the electrodes are manufactured by printed electronic technologies for usage in flexible and stretchable physiological monitoring devices, that are integrated into a shirt and eventually the IP signal is recorded with the same electrodes as ECG signal.

2.8.1 Impedance Pneumography Measurement System

Impedance pneumography measures changes in the electrical impedance of the person's thorax caused by breathing. The principle of IP measuring system follows Ohm's law and like every bio-impedance measurement system is based on the relationship between the injected current I to the tissue through electrodes and the measured voltage U between the electrodes, as $Z = U/I$.

IP is measured by feeding a high frequency AC current signal to thoracic area and measuring the voltage changes. This gives the impedance changes due to respiration such that inspiration typically results in an increased impedance. The increased impedance in inspiration is mainly due to an increase in air volume of the chest in relation to the fluid volume and an increase of conductance paths due to the expansion. The allowed amount of current by the ANSI/AAMI IS1-1993 standard is larger in higher frequencies. This signal acts as a carrier that is amplitude modulated by the respiration changes. Finally, it is demodulated to remove the high frequency component. The demodulation signal has the same frequency as the carrier with a phase shift to account for the phase delay in the signal path. This phase delay is important in the impedance measurement since an inappropriate amount of the phase shift results in a low demodulator gain and a poor extraction of the signal of interest. The first panel Figure 2.8 depicts a simulated 3 Hz square signal (low frequency carrier signal for the ease of illustration) which is modulated by a measured IP signal. The second and third panels illustrated the demodulated signal before and after filtering, respectively.

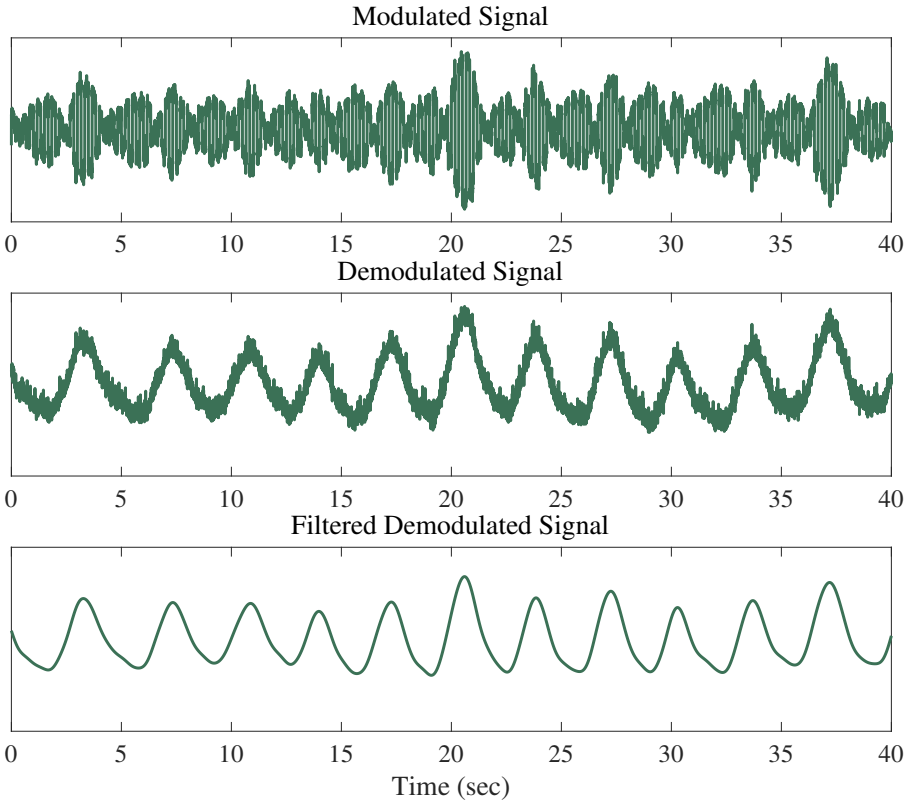

Figure 2.8 *Modulated, demodulated and filtered version of demodulated IP signal*

The IP is usually measured through 2- or 4-electrode measurement circuit. In the four configuration (tetrapolar), two electrodes are used for feeding the AC current and the other two are used for measuring the voltage changes. In the case of having only two electrodes, voltage is measured from the same electrodes used for applying the current. The two-electrode configuration introduces some errors due to the nonlinear voltage changes generated by current at the electrode-tissue interface. Using the four-electrode configuration minimizes the effect of this issue by having physically separated voltage measurement points and therefore, yields a more precise measurement [47]. Although in ambulatory devices with two electrodes for ECG monitoring, the bipolar IP technique is usually implemented since the tetrapolar technique requires two additional electrodes. However, in tetrapolar measurements in addition to the respiratory rate, tidal volume and respiration cycle length can also be observed and estimated [43]. Hence, there has been always a trade-off between bipolar and tetrapolar IP techniques. A comprehensive description of IP measuring system for respiration measurements has been written by Ville-Pekka Seppä in his

PhD thesis [48].

2.8.2 Respiratory Rate Estimation Techniques

A variety of digital signal processing methods have been proposed for estimating the respiratory rate. Autoregressive (AR) modeling have been widely used for estimation of respiratory rate. Nepal et al. [49] have developed an automatic algorithm for estimation of respiration rate and apnea detection. They have combined a second order autoregressive modeling and a modified zero-crossing technique for classifying the respiratory signal into three categories, apnea, respiration, or respiration with motion artifacts. Johnson and his colleagues [50] have been employed AR modeling for estimating respiratory rate from ECG signal. Karlen et al. [51] have introduced a method based on Fast Fourier Transform (FFT) for extracting respiration rate from PPG signal.

Autocorrelation function (ACF) that measures the similarity of a signal with itself at different points in time, has been applied in many physiological signal processing approaches for rate detection e.g. in ECG and PPG signals [52, 53]. This model is usually used for finding the repeated patterns in a signal such as respiratory rate. Sun and Matsui [54] have presented an autocorrelation model for a rapid and stable respiratory rate estimation from Doppler radar's signals. They considered the first peak after the midpoint of the auto correlation function (ACF) as the respiration rate from Doppler radar signals and then evaluated their method with a reference measurement that is the respiratory rate measured by a respiratory belt. They have shown that in autocorrelation technique the effect of body movement artefacts is decreased in comparison to the traditional approach. Above methods have been used for other physiological signals that carry respiration information as well. In this master thesis, the autocorrelation technique is used for estimating the respiratory rate from IP signals.

2.9 Other Physiological Signals

In this thesis work, a novel generic physiological signals classifier is proposed which has the ability for classifying five different physiological signals from each other. These signals are electrocardiography (ECG), impedance pneumography (IP), seismocardiography (SCG), electromyography (EMG) and photoplethysmography (PPG).

In above section, origin and characteristics of ECG and IP signals are described. Since, the other three signals are not included in DISSE project, no signal processing method was developed for them and they were used only for designing the classifier which is explained in details in chapter 3. In the following the basic definition of these three signals (SCG, EMG and PPG) are briefly explained.

2.9.1 Seismocardiography

Seismocardiography measures the cardiac vibrations induced by the heart beat. SCG contains information about the mechanical events of heart like heart sounds and cardiac output. SCG measurement system has been changed during the years due to development in accelerometer technologies. Current SCG measuring systems contain miniature accelerometers which are based on microelectromechanical technology. SCG signal is formed of several systolic and diastolic components. A comprehensive study about seismocardiography and its practical implementation and feasibility has been made by Mikko Paukkunen in his doctoral dissertation [55]. A short example of SCG signal is shown in Figure 2.9.

2.9.2 Electromyography

Electromyography records the electrical activity of muscles that helps in the diagnosis of neuromuscular abnormalities. Motor neurons send electrical signals to muscles and stimulates them. The stimulation produces electrical signals that lead to muscle contraction. There are two types of EMG measurement system: surface and intramuscular. In the surface method, the muscle activity is measured from above the muscle on the skin with surface electrodes. This method provides limited information of muscle activity although in intramuscular way, which is recorded by inserting needle electrodes into the muscle, more details and accurate information of the muscle are obtained [56]. A short example of EMG signal is shown in Figure 2.9.

2.9.3 Photoplethysmography

Photoplethysmography is a simple optical method for observing changes of blood volume in peripheral circulation. PPG is a low cost and non-invasive measurement

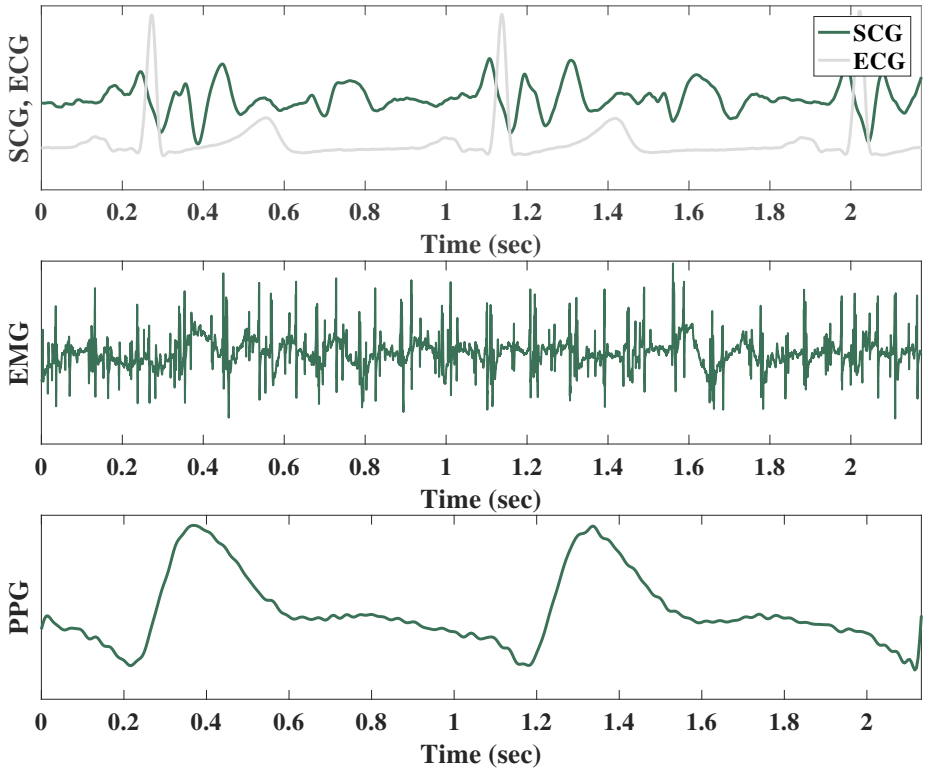

Figure 2.9 *These three physiological signals are used in the proposed classifier in addition to ECG and IP signal. A short example of these signals are plotted, from top to bottom SCG (ECG is shown in gray color for showing the periodicity of SCG), EMG and PPG.)*

that provides useful information about the cardiovascular system and widely used in clinical physiological measurement and monitoring. PPG measurement system contains high-intensity (usually green) light-emitting diodes (LED) and photodetectors that measure the intensity of light absorbed by blood. Wearable pulse rate monitoring devices are built in based on the same technology and detect the changes in light intensity that transmitted through or reflected from the tissue [57]. A short example of PPG signal is shown in Figure 2.9.

In Figure 2.9, top subplot shows SCG and ECG signals from one subject at the same time. The ECG signal is just shown for better observation of SCG periodicity in response to ECG signal. The middle subplot shows the EMG signal from tibialis anterior muscle of a healthy subject during dorsiflexion. The last one represents the PPG signal. These signals are obtained from databases that were used in designing the physiological signal classifier and their details information are provided in

chapter 3.

3. MATERIALS AND METHODS

In Figure 3.1, an overall view of the proposed automated approach from physiological signal classification to ECG and IP analyses, implemented in this thesis work, is illustrated. In this block diagram, our motivation toward developing an automated algorithm that can detect the measured signal and then automatically changes to the detected mode for the further analyzing and processing tasks is depicted. Furthermore, in the proposed automated algorithm, if an input signal is known, it automatically goes to its analysis section, otherwise it is passed through our proposed generic classifier to get known and then it goes to the processing part. In this thesis work, five different physiological signals were considered for classification part, but only for two of them (ECG and IP) different signal processing methods and techniques were developed and implemented.

All the signal processing methods and algorithms were implemented in MATLAB software (R2015b) from MathWorks Inc., Natick, MA, USA. In the following sections, first we go through the proposed robust physiological classifier and then the implemented analysis methods and processing techniques are presented.

3.1 Novel Generic Physiological Signals Classifier

Fig. 3.2 shows the architecture of the proposed physiological signal classifier that consist of data preprocessing, signals segmentation, feature extraction/selection and classification parts. For developing this classifier different databases were used that are described in section 3.1.1. It can be seen that used databases were divided into training and testing sets. Firstly, the training set is passed through all the steps of the classifier (pink arrows). Whenever the best performance was achieved, the classifier parameters are stored for evaluation phase. During evaluation phase (gray arrows), the testing set passes also through the same steps except the last one that is the learning phase (Modeling/ Learning block). Instead of that, the testing set is evaluated by a trained neural network (Detection/ Decision Making block). Each

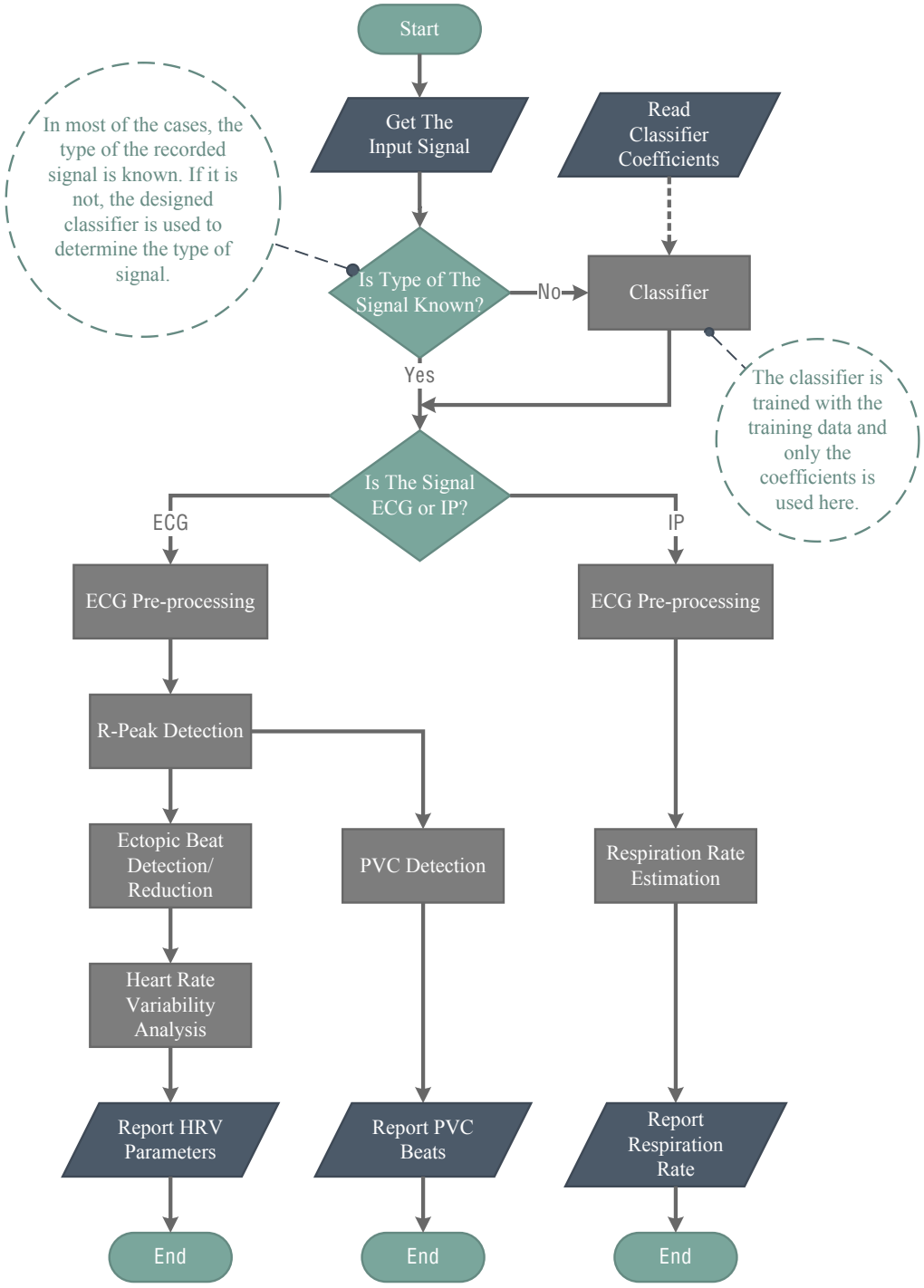

Figure 3.1 *An automated approach: from physiological signal classification to processing and analyzing ECG and IP signals, that is implemented in this master thesis. The classifier block is presented in 3.1 section, after the classifier section the left path corresponds to ECG processing and analyzing methods that presented in 3.2, and the right path, shows corresponding analysis methods for IP signal which described in 3.3.*

part of the classifier is described in details in the following sections.

3.1.1 Signal Database

Combined measurement of ECG, breathing and seismocardiogram (CEBS) Database

The measurements have been recorded by using a Biopac MP36 data acquisition system in supine position from 20 healthy volunteers. Each record lasts for about one hour. The CEBS database is publicly available at PhysioNet archive [58]. ECG signals from leads I and II were respectively measured thorough channels 1 and 2 of the system with a bandwidth between 0.05 Hz and 150 Hz. The channel 3 was devoted to measure the respiratory signal by using a thoracic piezo-resistive band with a bandwidth of 0.05 Hz to 10 Hz (since here, Resp corresponds to the respirarory signals measured by using a thoracic piezo-resistive band) and the channel 4 was used to obtain SCG using a triaxle accelerometer and a bandwidth between 0.5 Hz and 100 Hz. Each channel has been sampled at 5 kHz.

Electromyography

EMG signals were recorded by using Myontec measuring device. The signals were measured from front thighs and rear thighs of the healthy subjects during walking. The sampling rate of the measurement was 1 kHz. In addition, another database for EMG signals were also considered which data were acquired with a Medelec Synergy N2 EMG Monitoring System. A needle electrode was placed into the tibialis anterior muscle of each subject and the patient was supposed to dorsiflex the foot softly against the resistance. The EMG signals were then recorded for several seconds, at the point when the patient was relaxed and the needle electrode was removed. Three subjects were participated in this study that one of them was healthy and the two others had neuromuscular and neuropathy disease, respectively. The frequency rate of the signals was 4 kHz. This database is publicly available at Physionet archive [59].

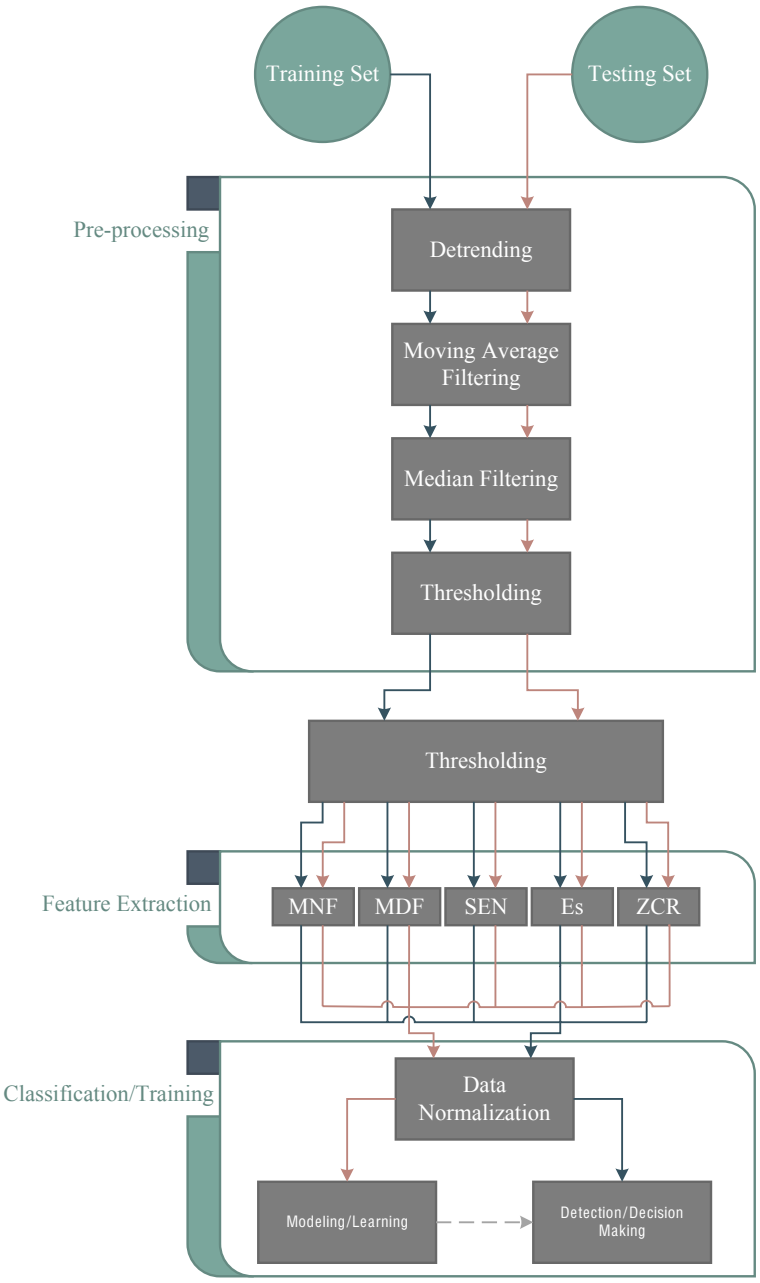

Figure 3.2 *An automated generic and robust architecture for physiological signals classification including three main steps: (1) Preprocessing, (2) Feature extraction and (3) Classification.*

Photoplethysmogram

PPG signals were collected from 19 subjects with the monitoring system proposed by Peltokangas et al. [60]. All the subjects were healthy male with age of 38.2 ± 13.1 years. The sampling rate of PPG signals were 500 Hz and the signals were recorded using wireless body sensor network (WBSN). These measurements have been done at department of Automation Science and Engineering of Tampere University of Technology.

Noisy Signals

In order to evaluate the influence of noisy environments on the performance of our generic classification algorithm, white Gaussian noise (WGN) were artificially added to a part of database which were used as the testing set. The level of noise was 0, 10 and 20 dB. WGN were added 10 times at each noise level to confirm the results. The signal to noise ratio (SNR) for each data is calculated by

$$SNR = 10 \log \frac{P_{clean}}{P_{noise}} \tag{3.1}$$

where P_{clean} is power of clean signal and P_{noise} is the power of WGN.

3.1.2 Data Preprocessing

An essential part of every pattern recognition system is preprocessing. In this work, preprocessing of the data consists of the following stages: detrending (baseline removal), moving average filtering, median filtering and thresholding. Since the aim was classification of different physiological signals which, have different bandwidths, then frequency based filtering methods were not applicable. In addition, since some parts of the used database in this project were obtained by wearable devices then occurrence of noise, motion artifacts and sensors error were inevitable. Therefore, the following filtering methods are applied on the signals to subtract their existing offset, reduce random noises and impulse interferences.

Detrending

Detrending methods can be used to remove a constant, linear, or curved offset from our signals if is present. Detrending methods fit a polynomial of a given order to the entire signal and simply subtracts this polynomial from the original signal. In this work, due to the restriction in applying frequency based filtering algorithms, detrending was a good choice for removing offset of our signals. The polynomial with order 6 was used for this approach.

Moving Average (MA) Filtering

MA filter works like a low pass filter which commonly used for smoothing and is an optimal choice for reducing random white noise. In biomedical applications, the MA filter is usually applied to reduce motion artifacts and works very good for a limited artifact range. Lee et al. [61] applied periodic moving average filter on PPG signals for removing motion artefacts. In MA filtering, each output sample is the average of M samples from the input signal at a time. The output is a convolution of the input signal with a rectangular pulse (with length M) having an area of one. MA filter is calculated as follow

$$y[i] = 1/M \sum_{j=0}^{M-1} x[i+j] \tag{3.2}$$

where M is the number of points in the averaging process which is set to 3 in this work, x is the input signal and y is the filtered output signal.

Median Filtering

Median filtering is applied on the signals to remove any possible spike, glitch or spike that might occur in the process of measurements due to digitization of analog to digital converter (ADC). The window size of five second is chosen in this algorithm.

Thresholding

One artefact in physiological signals measurement is large amplitude that exceeds a certain value. This artefact might be happened at the beginning of the measurement due to e.g. electrodes disattachment. Since our aim was proposing a generic automated algorithm that can classify raw unlabeled physiological signals into the correct categories, it was necessary to remove this artefact. Defining a certain threshold or thresholding the amplitude of the measured signal is a good solution for discarding this kind of artefacts. By assuming that our measured signals are enough long that have Gaussian distribution and artefacts cause strongly deviating values, setting threshold can be straightforward. By estimating the mean μ and standard deviation σ of the amplitudes in a signal, it can be expected that 99 % of the amplitude values are suited between $\mu - 3\sigma$ and $\mu + 3\sigma$. In this work, the interval $(\mu - 3\sigma, \mu + 3\sigma)$ was chosen as the thresholding value for each signal's amplitudes.

3.1.3 Feature Extraction/Selection

Signals Segmentation

After preprocessing section, each signal was segmented into 10-second frames. Every 10-second frame of the signals was used in feature extraction section. In below steps, some features were extracted from every preprocessed 10-second frames of our database. Then these features were used as the training data and test data of the classifiers.

Mean Frequency (MNF)

MNF is an average frequency which is calculated as the sum of product of the frequency and the signal power spectrum, divided by the total sum of the power spectrum. MNF commonly referred to centroid frequency were used as a feature for EMG and ECG classification in [62] and [63], respectively. It can be defined as

$$MNF = \sum_{j=1}^{M} f_j P_j \Big/ \sum_{j=1}^{M} P_j \tag{3.3}$$

where f_j is the frequency value of signal power spectrum at frequency bin j, P_j is the signal power spectrum at frequency bin j, and M is the length of frequency bin.

Median Frequency (MDF)

MDF is a frequency at which the signal power spectrum is divided into two regions with equal amplitude which also were used as a feature for a robust EMG classification system by Phinyomark et al. [62]. It can be expressed as

$$\sum_{j=1}^{MDF} P_j = \sum_{j=MDF}^{M} P_j = \frac{1}{2}\sum_{j=1}^{M} P_j. \tag{3.4}$$

Spectral Entropy (SEN)

SEN is a normalized form of Shannon's entropy which uses power spectrum amplitudes components of the time series for entropy evaluation [64]. Shannon Entropy (ShEN) of a signal is the measure of set of relational parameters that vary linearly with the logarithm of the number of possibilities and describes its average uncertainty [65]. SEN can be calculated as follow

$$SEN = -\sum_{j=f_{low}}^{f_{high}} P_j \log P_j \Big/ \log N_f \tag{3.5}$$

where f_{low} and f_{high} are the lowest and highest frequencies in the spectrum, respectively. N_f is the number of frequency bins.

Energy (E_s)

Energy E_s of a discrete-time signal $x(t)$ is defined as

$$E_s = \sum_{-\infty}^{\infty} |x(t)|^2 dt. \tag{3.6}$$

In this work, the energy E_s for each 10-second segment of the data was calculated and used as an input to the classifier.

Zero Crossing Rate (ZCR)

ZCR refers to the number of times that the amplitude values of a signal pass the zero y-axis and it presents an approximation of frequency domain properties of the signal. It can be expressed as follow

$$ZCR = 1/N \sum_{n=2}^{N} |sign(x(n)) - sign(x(n-1))|. \tag{3.7}$$

3.1.4 Classification Method: Neural Networks (NN)

From previous section, five general purpose features were extracted from every segmented frame of our signals (which were ECG lead I, ECG lead II, Resp, SCG, EMG from thigh, EMG from anterior tibia and PPG). These five features of each frame were considered as one feature vector in the training or testing phase of the classifier. The number of feature vectors were 4934, 4934, 5017, 4934, 1800, 1946 and 5253 for ECG lead I, ECG lead II, Resp, SCG, EMG from thigh, EMG from anterior tibia and PPG signals, respectively. These feature vectors were placed into a matrix and created the neural network dataset.

Neural network is one of the most popular modeling methods which is used in the medical research fields [66]. The NN learns the labeled classes of the database by modeling the training data and compares them with the predicted classes with the purpose of modifying the network weights for the next iterations of training [67]. Different steps of the classification method are described as follow:

Feature Normalization

Data normalization is an essential part of each pattern recognition systems. This step is very important when dealing with parameters of different units and scales. By normalization, the feature matrix will have zero mean and unit variance that can be calculated as $x_{norm} = \frac{x-\mu}{\sigma}$, which x and x_{norm} are the original feature matrix and normalized one, respectively. μ is mean and σ is standard deviation of the feature matrix.

Modeling/Learning phase by NN

First of all, our feature matrix was randomly divided into three subsets by different ratios. The first subset included 70% of the feature matrix that was assigned to the training set, the second and third subsets with equally 15% of the feature matrix were assigned to the validation set and testing set, respectively. The layers of NN consist of X input neurons, N hidden neurons and Y output neurons. Where X is equal to the number of feature vectors of the training set, N has been set to 15 heuristically, and Y is equal to 7 that represents seven different physiological classes that were considered in this classifier including ECG lead I, ECG lead II, Resp, SCG, EMG (from tibialis anterior), EMG (from thigh) and PPG signals. The sigmoid transfer function was selected and for the training of the weights, back propagation method was used.

The error between the network outputs and the target outputs on the training set was calculated during the learning phase. In addition to that, the error on the validation set was also monitored in order to determine when overfitting has begun. The validation and training set errors usually decrease at the beginning of the training phase but the validation error begins to rise if the network starts to overfit the data. The network weights and biases were saved at the minimum of the validation set error. In addition to error rate, the percent error (PE), fraction of samples that were misclassified, was also determined as an evaluation factor. The training process (with different initial weights and biases) was repeated 10 times and the parameters were saved for the decision making phase when the lowest percent error was obtained; In other words, when the least misclassification happened in the learning phase.

Detection/Decision Making phase by NN

Testing set was used for evaluating the performance of our model (trained NN) in response to unseen data with and without occurrence of noise. WGN with level 10 and 20 dB were artificially added to the original database (raw database) and then all the steps of the block diagram in Fig 3.2, were applied on the noisy signals (gray arrows). Eventually, parts of noisy signals which had the same indexes as testing set were evaluated in the result chapter. WGN were added 10 times to the signals to confirm the results. Finally, the average PE values of the testing set with 0, 10

and 20 dB WGN were calculated and analyzed. The performance of the classifier is presented in chapter 4.

It should be mentioned that the novel generic physiological signals classifier proposed in this master thesis work is also published and presented in XIV Mediterranean Conference on Medical and Biological Engineering and Computing 2016 [68].

3.2 ECG Signal Analysis

The ECG analysis path is expressed in the bottom left part of the block diagram shown in Figure 3.1. Over the past thirty years, different algorithms were proposed for ECG signal analysis and some of them have achieved better accuracy than the others. Although none of them has presented a result with 100% accuracy. A few of them are selected in this work according to their presented results. This chapter describes the materials and methods used for ECG analysis within this work. Firstly, all the used materials are introduced. Then selected digital signal processing (DSP) methods are described.

3.2.1 ECG Database

We needed databases which include sets of annotations for each recording to evaluate our developed algorithms. Annotations are referred to specific points of a recording and describe events at those locations. For instance, for ECG signals, annotations indicate the times of occurrence and types of event.

MIT-BIH Arrhythmia Database MIT-BIH Arrhythmia database was chosen for evaluating our implemented analysis techniques. This database contains 48 half-hour of two-channel ambulatory ECG recordings. The database was recorded with sampling rate 360 Hz per channel with 11-bit resolution. Two or more cardiologists independently annotated each record; disagreements were resolved to obtain the reference annotations for each beat included with the database. This database is publicly available [5].

3.2.2 Pre-processing Methods

In ECG analysis path of the block diagram in Figure 3.1, the first step is referred to preprocessing; since the ECG signals may be corrupted by different types of noises/artefacts such as power-line interference, motion artefacts and muscle contractions.

Power-line Interference Rejection

The most common form of noise is power-line interference and its harmonics [69]. Using single or multiple notch filters are the simplest ways for removing this form of noise from measured signals [70]. Although, when using conventional digital filtering, beginning of the signals, which might include some significant information, is entirely lost due to transient state of the filter. In this work, we applied a modified notch filter with transient suppression method called vector projection which prevents any transient response at the beginning of filtered signal [71].

In 1995, Pei and Tseng introduced vector projection to find non-zero initial conditions for IIR notch filter [72]. In this method, first, vector projection is applied to break down the first M samples of noisy signal into two parts; clean (desired) and sinusoidal interference parts. Then, the clean part is used as initial values for the traditional notch filter. The algorithm is explained in following. First, the input data is arranged as vector $X = \begin{bmatrix} x(0) & x(1) & \cdots & x(M-1) \end{bmatrix}^T$, then matrix A is constructed as

$$A = \begin{bmatrix} 1 & \cos(\Omega_0) & \cdots & \cos((M-1)\Omega_0) \\ 1 & \sin(\Omega_0) & \cdots & \sin((M-1)\Omega_0) \end{bmatrix}, \tag{3.8}$$

and projection matrix P is computed as

$$P = A(A^T A)^{-1} A^T. \tag{3.9}$$

The first M samples of the output signal are then obtained by

$$Y = \begin{bmatrix} y[0] & y[1] & \cdots & y[M-1] \end{bmatrix}^T = QX, \tag{3.10}$$

where $Q = (I - P)$ and I is identity matrix. The rest of the signal samples, which are samples M to $N-1$, can be calculated by Equation (3.11) which is the transfer function of a second order IIR notch filter with pole radius r and notch frequency Ω_0.

$$H(z) = \frac{1 - 2\cos(\Omega_0)z^{-1} + z^{-2}}{1 - 2r\cos(\Omega_0)z^{-1} + r^2 z^{-2}} \cdot \tag{3.11}$$

According to [73], the length of the input vector should cover the period of power-line fundamental frequency to achieve the optimal non-zero initial conditions for the notch filter. This indicates that with higher sampling rate a longer window of input samples is needed to reconstruct the noise accurately.

Baseline Wander Removal

Baseline wander removal has been one of the very first challenges in ECG signal processing [74]. There are two common techniques for removal of baseline wander that are linear filtering and polynomial fitting (that is also called de-trending). In this thesis work, we first applied a linear, time-invariant high-pass filter on the signal. The cut-off frequency is set to 0.2 Hz so that the clinical information in ECG remain unchanged. And for preventing any phase distortion, finite impulse response (FIR) high-pass filter is selected. Unfortunately, filtering based techniques cannot remove baseline wander that occur e.g. due to stress or body movement. Therefore, we also applied polynomial fitting technique to diminish the amount of baseline wander as much as possible. This method, fit a polynomial of a given order to the entire signal and simply subtracts this polynomial from the original signal. A polynomial with order 6 was used for this approach.

Muscle Noise Removal

An appropriate way for removing high frequency muscle noises is low-pass filtering. As it is mentioned in 3.2.2 part, here also FIR low-pass filter is designed to prevent any phase distortion on the filtered signal. Cut-off frequency of the low-pass FIR filter is set to 200 Hz.

Thresholding

As it is mentioned in the section 3.1.2, one of common artefacts in physiological measurements is occurrence of large amplitude that is usually happened at the beginning of the measurement due to e.g. electrode dis-attachments. By defining a threshold, we can get rid of this type of artefact. Choosing the threshold value is straightforward and can be selected in an adaptive manner. To be more precise, for each specific signal which is enough long that we can assume the measured signal have Gaussian distribution, the threshold value is chosen based on mean μ and standard deviation σ of the signal amplitudes. It is expected that 99 % of the amplitude values are suited between $\mu - 3\sigma$ and $\mu + 3\sigma$. Those parts of a signal that exceed this interval $(\mu - 3\sigma, \mu + 3\sigma)$ will be automatically removed.

3.2.3 R-peak Detection Techniques

Accurate R-peak detection is an important step in every ECG analysis tasks. A variety of methods have been proposed in the past years, here we implemented one of the well-known method [28], its modified version [75] and also an accurate R-peak detection for telemedicine [76] and then compared their results with the annotated file available in database.

Pan-Tompkins QRS Detection Algorithm

The well-known QRS detection algorithm proposed by Pan and Tompkins in 1985 was applied on ECG signals to detect the R-wave fiducial points [28]. The Pan-Tompkins method recognizes QRS complexes based on analyses of the slope, amplitude, and width. The algorithm includes filtering, derivative, squaring and integration steps. First of all, a band-pass filter reduces the impact of T wave and remove baseline drift and power-line interferences, if present. Then, derivative procedure suppresses the low frequency components such as P and T waves, and provides a large gain to the high-frequency components arising from high slopes of QRS complex. The squaring operation re-emphasizes on high-frequency components in the signal that related to QRS complex. At the end, the squared waveform passes through a moving window integrator. Since rising edge of the integration waveform corresponds to QRS complex then the fiducial point can be determined as the peak

of the R-wave [28, 77].

Pan-Tompkins Algorithm with Optimal FIR Band-pass Filter

Schlindwein et al. [75] in 2006 proposed some optimal values for center frequency and bandwidth of Pan-Tompkins's band-pass filter. They performed an exhaustive search for center frequencies ranging from 13 to 20 Hz and for band-widths from 5 to 12 Hz, at integer values of 1 Hz for both. They applied the new FIR band-pass filters on MIT-BIH Arrhythmia database and chose the optimal values based on produced minimum number of errors i.e. sum of false-positives and false-negatives (according to the available annotations from database). The optimum point was found at center frequency 19 Hz and bandwidth 9 Hz.

Area-based R-Peak Detection Algorithm

The method proposed by Liao et al. [76] is an area-based approach based on the fact that QRS complexes are very narrow and tall which result in large areas over the curve around QRS complex locations. The motivation of this method is come from the fact that if the amplitude of T-wave is even higher than R-peak, QRS complex is still recognizable due to its narrow and tall morphological characteristics. In this method, it is considered that the typical QRS complex is last up to 120ms, then for each local maximum M, N neighbors have been chosen as the set of points within 60ms from M. Then, M's area over the curve is defined as the sum of the magnitude of M minus the magnitude of every point in N. The peaks are then sorted by their area under the curve, and those with the greatest areas are considered as R-peaks.

After obtaining R points from above R-peak detection methods, the detected R fiducial points from each individual method are compared to the annotated R points in every signals of database. The evaluation method was based on number of missed detected points and false alarms. The R-peak detection method that results in highest sensitivity and lowest false alarm was chosen as the best one and its output is used for further steps. The evaluation method is presented in section 3.2.9.

Eventually, by obtaining the R-wave fiducial points from the best R-peak detection method, the RR intervals for each signal were calculated as the time intervals between each two successive R peaks of the ECG.

3.2.4 Ectopic Beats Detection

The goal of this section is recognition of ectopic beats from normal beats. In this section, we used morphological features of R-peaks of ECG to find out time of occurrence and type of ectopic beat. Firstly, we applied a simple morphological technique to distinguish ectopic beats from normal ones. This technique is based on evaluating the RRIs duration and amplitude of R-peak [78]. In this method, the current RRI (RR_i) is compared to the running average of the last six normal RRIs (RR_m). Then according to three rules presented in Equation 3.12, current heartbeat is considered as an ectopic or a normal beat.

The first condition says that, if the value of current RRI (RR_i) is less than 85% of RR_m; it is too short for a normal heartbeat then the current heartbeat is considered as abnormal. For the second condition, if the value of (RR_i) lies within $90-110\%$ of (RR_m), the current heartbeat is considered as normal. Finally, for the third condition, if the amplitude of current R-wave (RR_i) lies within $60-130\%$ of average value (R_m), the heartbeat is classified as a normal one, otherwise it is marked as an abnormal beat. In this technique, we assumed that the first six heartbeats were normal.

$$
\begin{aligned}
1st\,condition: &\begin{cases} if\ \ RR_i < 85\%\, RR_m,\ \ then\ abnormal \\ else,\ normal \end{cases} \\
2nd\,condition: &\begin{cases} if\ \ 90\%\, RR_m < RR_i < 110\%\, RR_m,\ \ then\ normal \\ else,\ abnormal \end{cases} \\
3rd\,condition: &\begin{cases} if\ \ 60\%\, R_m < R_i < 130\%\, R_m,\ \ then\ normal \\ else,\ abnormal \end{cases}
\end{aligned}
\tag{3.12}
$$

After detection of ectopic beats with the simple morphological based method, for every subject of MIT-BIH Arrhythmia database, the heartbeat was marked as normal or abnormal. Then the accuracy of the ectopic beat detection method was evaluated with the annotated file from the database. In this works, all the annotations related to ectopic beats and premature beats were considered for evaluating the ectopic detection method. The evaluation method is based on the confusion matrix presented in Figure 3.6 in evaluation 3.2.9 section.

3.2.5 Ectopic Beats Reduction

Many algorithms have been developed for correcting the ectopic beats in heart rate and HRV analyses. In fact, the effect of ectopic beats on heart rhythm can be corrected by removal or replacement process. The simplest method is deletion that removes all ectopic beats from ECG signal and subsequently, normal beats are shifted which results in shorter ECG signal. Therefore, deletion method can alter time, frequency and non-linear parameters of the signal. The method used in this work called interpolation of zero degree. This method is useful when the occurrence of ectopic beats is very occasional. In this technique, ectopic beats are replaced by the average of N surrounded normal beats. It can be calculated by given formula

$$RR_{new}(t) = \frac{1}{N}\sum_{i=1}^{N} RR(i) \tag{3.13}$$

where $RR_{new}(t)$ is the corrected value of the detected ectopic beat. In this work N is set between 3 and 10.

3.2.6 Heart Rate Calculation

For heart rate analysis, the corrected RR interval obtained from previous step is used. Heart rate can be calculated from following formula

$$HeartRate = 60/RR\,Interval, \tag{3.14}$$

in which, $RR\,Interval$ is the time interval between each two consecutive R peaks of the ECG signal that is represented in seconds. Therefore, the unit of $HeartRate(HR)$ is beat per minute (bpm).

3.2.7 Heart Rate Variability Parameters

Heart rate variability analysis has become a non-invasive tool for studying the operation of autonomic nervous system. The analysis of beat-to-beat heart rate can be approached in several ways such as time domain analysis, spectral analysis and

non-linear analyses. In this work, some widely used linear and non-linear time domain parameters were calculated. The parameters were implemented based on their standard definitions in [79] as following:

- SDNN: Standard deviation of all RR intervals
- RMSSD: Root mean-square of successive differences of adjacent RR intervals
- pNN50: Percentage of pairs of adjacent RR intervals differing by more than 50 ms from all RR intervals
- SD1: Standard deviation of data against the axis x = y in Poincaré plot
- SD2: Standard deviation of data against the axis, which is orthogonal to the axis x = y in Poincaré plot (crosses this axis at the mean value of the data)

Poincaré plot is constructed by plotting the RR intervals as a function of itself with a delay of 1 sample. The accuracy and precision of HRV parameters that were computed by implemented methods were validated with Kubios software, which is an open license HRV analysis software developed in University of Kuopio, Finland. [80].

3.2.8 PVC Detection Algorithms

During a PVC beat, ventricular contraction happens earlier than usual which means the R-peak appears earlier. Hence, RR intervals of PVCs are smaller than normal heartbeats. According to the second condition in Equation 3.12, initially normal and ectopic beats are distinguished from each other, then the PVC algorithm determines the occurrence of PVC beats beyond the detected ectopic beats. As mentioned earlier in section 2.7.2 and shown in Figure 2.7, there are two typical shapes of PVC beat. Chang et al. [39] have proposed a PVC detection algorithm that can detect both types of these PVC beats. Their algorithm is a combination of two methods that are called sum of the trough, and sum of the R-peak with minimum. Both methods that are defined based on morphological features of PVC beats are implemented in this thesis work.

Sum of Trough

Chang and his colleagues proposed Sum of Trough method for a PVC beat that has below morphological features:

1. The RRI is smaller than the mean RRI; ($RR_i < RR_m$).
2. There is a huge and wide negative wave after R-peak.
3. There is a big pause before beginning of the next heartbeat.

According to above characteristics, they have summarized their method in below formula

$$sum = \sum_{n=k_1}^{k_2} x[Rpoint[i] + n] \tag{3.15}$$

where function x represents the amplitude of the ECG signal, *Rpoint* correspond to the location of R-peak and n is the number of samples after R-peak which is set to range $35 : 85$ by Chang et al. If the *sum* value is smaller than a threshold, this method detects the occurrence of PVC. Figure 3.3, presents the logic of this PVC detection method very well that is saying if the summation of n samples (indicated with a pink arrow) after R-peak (light green stars) is smaller than a threshold (dashed pink line), the algorithm determines the beat as a PVC. The left y-axis corresponds to amplitude of ECG and the right y-axis corresponds to the threshold values. Since the threshold value was not defined by Chang and his colleagues, we have studied the outcome of this algorithm with different threshold values. In addition to that, the range of n was also experimentally studied in this work.

R-peak with minimum

This method covers the other typical type of PVC beats that have the following characteristics

1. The RRI is smaller than the mean RRI; ($RR_i < RR_m$).

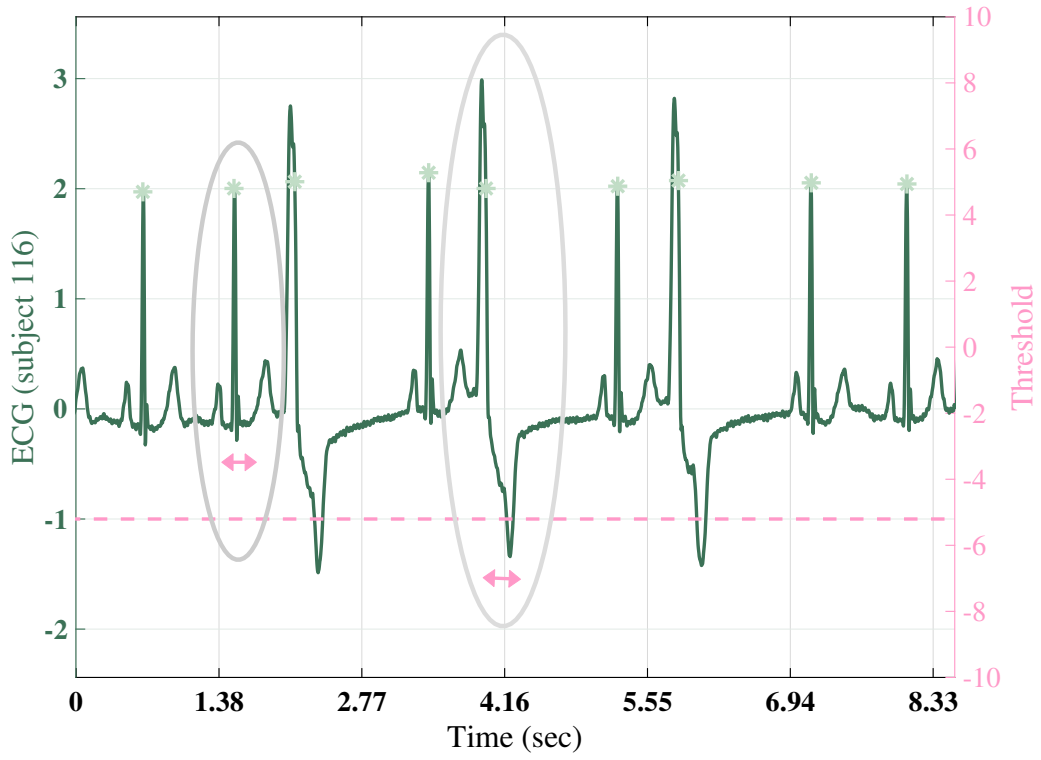

Figure 3.3 *PVC detection Algorithm: Sum of Trough, that is based on summation of n samples after R-peak (light green stars). Whenever this sum value is smaller than a threshold (e.g. dashed pink line), the algorithm determines the beat as a PVC otherwise marks it as a normal beat. The left y-axis corresponds to amplitude of ECG and the right y-axis corresponds to the threshold values.*

2. The R-wave amplitude is mostly smaller than R-wave in normal beats.
3. There is a huge and narrow negative wave after R-peak.
4. There is a big pause before beginning of the next heartbeat.

According to above characteristics, they have derived the below formula for detecting this kind of PVC beats.

$$diff = min + x[Rpoint[i-1]] \tag{3.16}$$

whereas, min is the minimum value between two consecutive R-peaks, function x represents the amplitude of the ECG signal and $Rpoint$ correspond to the location of

R-peak. If the $diff$ value is less than a threshold; which was set to zero by Chang et al., the system marks the beat as a PVC. For this method, we also evaluated outcome of the algorithm with different values for the threshold. Figure 3.4 illustrates how diff value (summation of pink arrows for each individual beat) is calculated for every beats of ECG signal and if it is smaller than a threshold, the algorithm detects the corresponding beat as a PVC. The left y-axis corresponds to amplitude of ECG and the right y-axis corresponds to the threshold values. One normal and one PVC beats are shown with a gray ellipse around them.

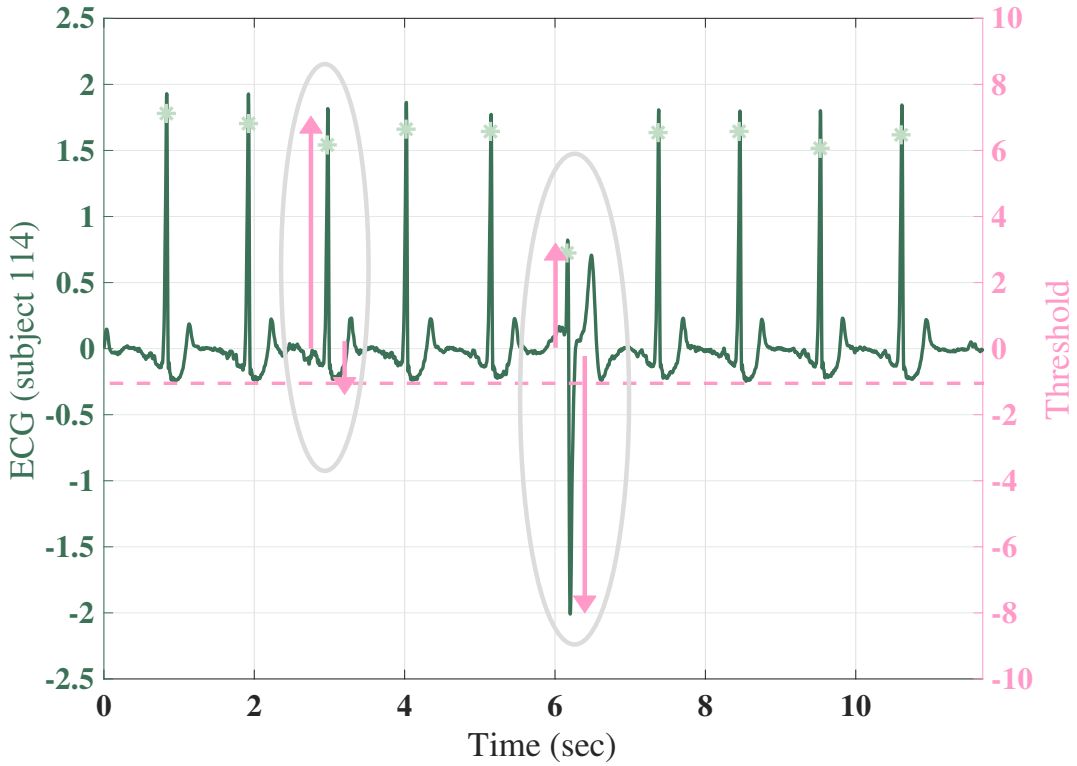

Figure 3.4 *PVC detection method: R-peak with minimum, if the diff value computed from the formula is smaller than a threshold, the algorithm detects the corresponding beat as a PVC. The left y-axis corresponds to amplitude of ECG and the right y-axis corresponds to the threshold values.*

3.2.9 Evaluation Methods

QRS Detection Methods

For evaluation of the QRS detection algorithms, the following scores for each QRS complex in the ECG records were calculated: TP, the true positive for QRS detec-

tion, i.e., the number of correctly detected R-peaks; FN, the false negative for QRS detection, i.e., the number of missed R-peaks; and FP, the false positive for QRS detection, i.e., the number of false R-peaks. These scores are gathered in confusion matrix of Figure 3.5 and obtained by comparing the results of our algorithms with the annotations file included in the database. According to the confusion matrix, actual classes correspond to annotation file which here positive classes are referred to the location of R-peaks and negative classes are corresponded to rest of the ECG signal. The same principle is considered for predicted classes which are the results of our QRS detection algorithms.

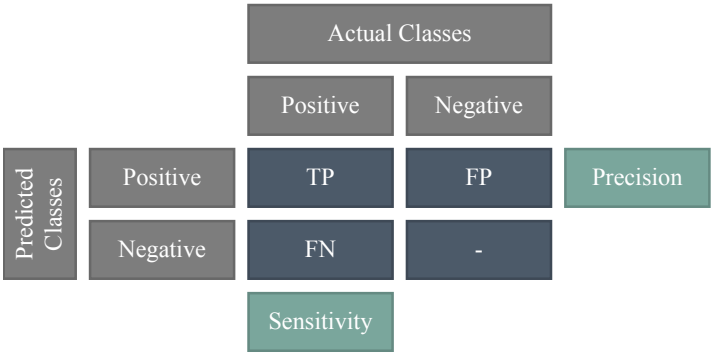

Figure 3.5 *Confusion matrix for evaluating QRS detection algorithms, TP: true positive, FP: false positive and FN: False negative*

Then we calculated standard performance measures; sensitivity and precision, for evaluating the QRS detection algorithms based on given formula

$$Sensitivity = \frac{TP}{TP + FN}, \quad Precision = \frac{TP}{TP + FP} \tag{3.17}$$

in which, TP, FP and FN are corresponding to true positive, false positive and false negative, respectively.

Ectopic Beat Detection

For evaluation of the ectopic detection method, following additional scores for each heart beat are calculated: TP, the true positive for ectopic detection, i.e., the number

of correctly detected ectopic beats; FN, the false negative for ectopic detection, i.e., the number of missed ectopic beats; FP, the false positive for ectopic detection, i.e., the number of false ectopic beats and TN, the true negative for ectopic detection, i.e., the number of correctly detected normal beats. These scores are gathered in confusion matrix of Figure 3.6 and obtained by comparing the results of the morphological based ectopic detection method with the annotations file included in the database. According to the confusion matrix, actual classes correspond to real types of ECG beats based on their annotation file which here positive classes are referred to ectopic/premature beats and negative classes are corresponded to normal beats of ECG signal. The same principle is considered for predicted classes which are the results of our ectopic detection method.

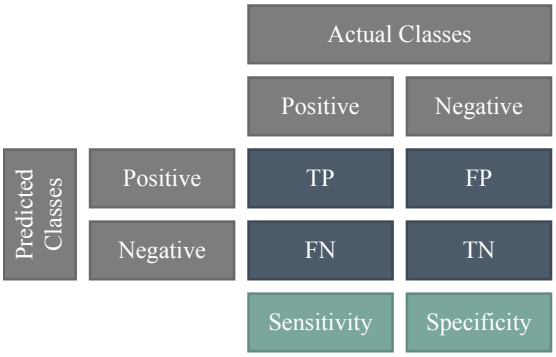

Figure 3.6 *Confusion matrix for evaluating ectopic detection method, TP: true positive, FP: false positive, FN: False negative, TN: true negative*

Then we calculated standard performance measures; sensitivity and specificity, for evaluating the ectopic beat detection method based on given formula

$$Sensitivity = \frac{TP}{TP + FN}, \quad Specificity = \frac{TN}{TN + FP} \tag{3.18}$$

in which, TP, FP, FN and TN are corresponding to true positive, false positive, false negative and true negative, respectively. High sensitivity shows how well ectopic beats can be distinguished from normal beats and high specificity presents low number of false alarm detected by implemented method.

PVC Detection Algorithms

For evaluating the implemented PCV detection method, receiver operating characteristic (ROC) or ROC curve is applied to illustrate the performance of PVC detection method when its discrimination threshold is varied. Sensitivity and specificity values were computed for every threshold values and then the ROC curve is plotted as a function of sensitivity and 1-specificity. The range of threshold for Sum of Trough method was chosen between -100 to 100 with a step of 0.01. In addition, for exploring the optimal range of n (number of samples after R-peaks that must be summed), different ROC curves were plotted and their area under the curves (AUC) were computed. The ROC curve which resulted in bigger AUC was chosen as the best range of n. The other PVC detection method, R-peak with minimum, were evaluated according to its ROC curve in a similar approach but its threshold was varied between -10 and 10 with a step of 0.01.

3.3 IP Signal Analysis

3.3.1 IP Database

IP signals were measured from 15 subjects (10 males and 5 females) in sitting position. The signals were recorded by two devices, one for measuring the IP and the other for monitoring the changes in the temperature of respiration using an NTC thermistor placed inside a mask that was worn in front of the mouth and nostrils. The temperature device was considered as a reference which provides a clean artifact-free signal. For more information about measurement procedure refer to the work by Jeyhani et. al. [81].

3.3.2 Data Pre-processing

According to Jeyhani et. al. [81] the range of respiration rate is considered between 4 to 60 breath per minute (bpm) and therefore the signals were filtered by a high pass Butterworth filter with cut-off frequency of 0.06 Hz and a low pass filter with a cut-off frequency of 1 Hz. The filtering was done by forward-backward technique to eliminate the effect of the non-linear phase of IIR filters.

3.3.3 Respiration Rate Estimation Methods

Respiration rate can be calculated from IP signal by the means of simple signal processing techniques. For this purpose, first the filtered signal is divided into 15-second long frames with 10 seconds overlap and the ACF was calculated for each frame. Next, a peak detection function is applied to detect the desired peak in the output of the ACF. The autocorrelation function of a periodic signal represents the same cyclic behavior of that signal. ACF is defined as

$$r(\tau) = \sum_{n=1}^{N-1-\tau} x(n)x(n+\tau), \tag{3.19}$$

where $x(n)$ is one frame of the signals and τ is the lag. Next, the first peak after the midpoint in ACF was detected and its lag multiplied by $60/f_s$ was considered as the respiration rate in bpm. The minimum horizontal distance for the peak detection procedure was set to 1s which is according to the respiration rate range considered.

The respiration rates were estimated from both of the signals (IP and the one acquired from the mask) and the results were compared. The results were evaluated by the means of mean absolute error (MAE) and root mean square error (RMSE) which are defined as

$$MAE = \frac{1}{N}\sum_{n=1}^{N} |\hat{y}[n] - y[n]| \tag{3.20}$$

and

$$RMSE = \sqrt{\frac{1}{N}\sum_{n=1}^{N} (\hat{y}[n] - y[n])^2}, \tag{3.21}$$

respectively. MAE can be seen as linear score of the magnitude of the individual errors without considering their direction and each with equal weights. RMSE on the other hand, gives relatively large weight to large errors (since the squaring is done before averaging). RMSE, which has a value larger than or equal to MAE, can give information about the variance in the error point. This can be observed as the difference between RMSE and MAE.

Figure 3.7 depicts the result of filtering and estimation of the respiration rate. The

first panel shows a 15-second frame of the IP measurement from one of the subjects. The second panel shows the effect of filtering and the period estimated by only peak detection in each cycle of the signal. Although, this method provides an easy and cycle-to-cycle estimates of the respiration rate, in most of the cases in which the respiration signal is not clean enough it is prone to be misled by the artifacts. The last panel shows the ACF, its midpoint and the first peak detected after that. This value is calculated from each frame of IP signals and temperature signal measured from the mask and the results are compared to evaluate the agreement between the two measurements.

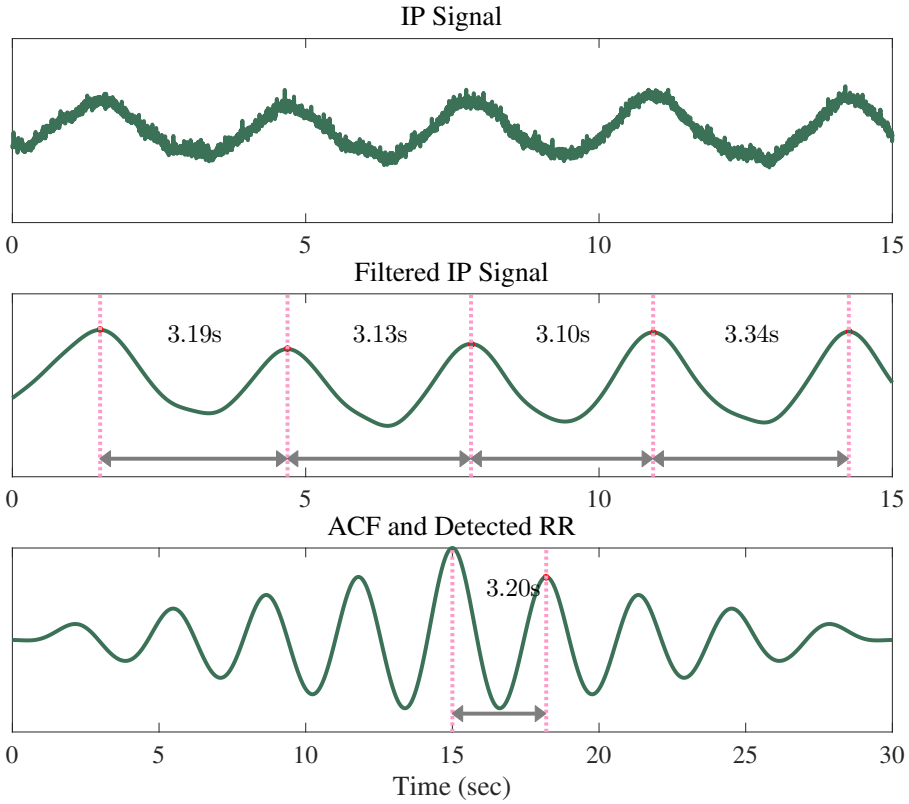

Figure 3.7 *Filtering and respiratory rate estimation by AFC. The top panel shows the original IP signal, the middle one shows the filtered IP signal and the panel in the bottom shows the ACF that its first peak after the mid-point is chosen as the respiratory rate.*

4. RESULTS AND DISCUSSIONS

In this chapter, results of the proposed classifier and then the implemented signal processing methods are presented, respectively.

4.1 Novel Generic Physiological Signals Classifier

Figure 4.1 illustrates performance plot of the proposed physiological signal classifier. The performance plot shows value of Cross-Entropy versus iteration number for training, validation, and test (with 0 dB noise) sets. Cross-Entropy presents the network performance based on the mean of error between the network outputs and the target outputs in logarithmic scale. The intersection point of green dashed lines (Best), indicates the time when validation set had the minimum error and the network weights and biases values were saved for the evaluation phase. The best validation error was 0.029384 and achieved at epoch 112.

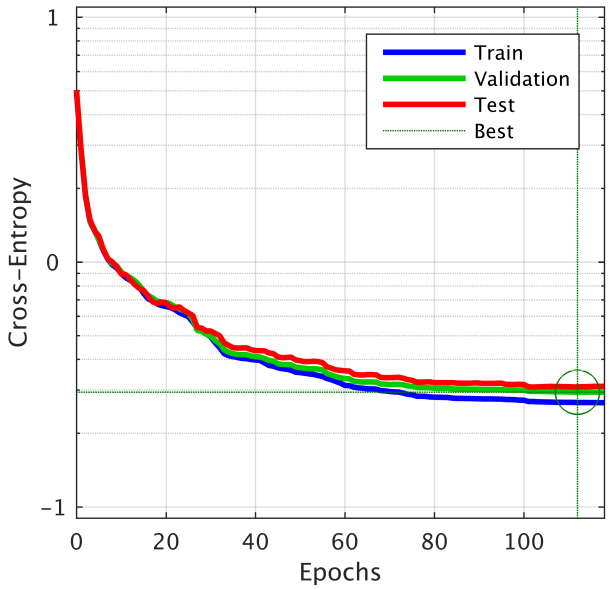

Figure 4.1 *Performance plot of NN for training, validation and testing sets.*

Figure 4.2 illustrates the confusion matrix of our network output which the rows show the predicted classes, and the columns show the true classes. The diagonal cells show where the true classes and predicted classes match. The off diagonal cells show instances where the classifier had made mistakes. The column on the right hand side of the matrix shows the accuracy for each predicted class, while the row at the bottom of the matrix shows the accuracy for each true class. The cell in the bottom right shows the overall accuracy (obtained by summation of diagonal cells divided by all) which is equal to 92.7%.

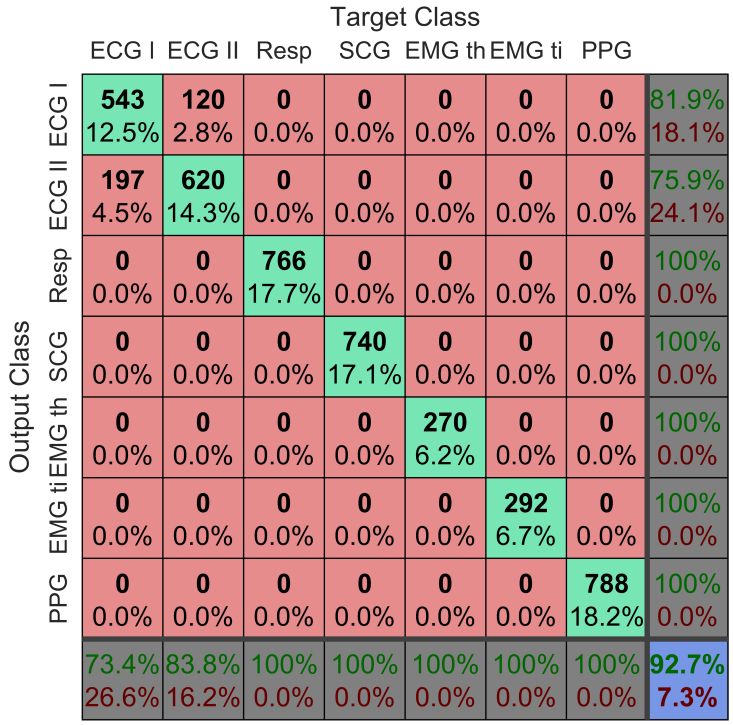

Figure 4.2 *Confusion matrix of the network outputs. The rows show the predicted classes and the columns show the true classes. The column on the right and the row at the bottom show the accuracy for each predicted class and each true class, respectively and the cell in the bottom right, presents the overall accuracy which is equal to* 92.7%.

It can be seen that the proposed generic classification algorithm was able to distinguish ECG (lead I and II), Resp, SCG, EMG (from anterior tibia and thigh) and PPG signals from each other with 100 % accuracy. The only exception was for ECG lead I and II which there were less than 27% error. It means that used

Table 4.1 *The average of percent errors for testing set with different levels of white Gaussian noise*

Test set	Average of PE (%)
with 0 dB WGN	7.60
with 10 dB WGN	8.76
with 20 dB WGN	8.88

general purpose features where enough discriminating to recognize different physiological signals from each other. However, for classifying ECG signals obtained from different leads or different locations, more specific ECG based features are needed.

Table 4.1, represents the average of PE (fraction of samples that were misclassified) were obtained from test sets with different level of white Gaussian noise. Results displayed in Table 4.1 indicate our generic classifier works quite robust in the noisy environments.

With the proposed classifier we were able to distinguish these five different physiological signals (ECG, EMG, SCG, Resp and PPG) from each other with 100 % accuracy. Although for distinguishing different leads of ECG, certain additional features are required. Eventually, it can be reported that the proposed generic classification algorithm has an excellent discriminatory power for classifying these different physiological signals from each other.

4.2 ECG Analysis

Pre-processing Figure 4.3 illustrates an example of noisy ECG signal and the effect of filtering on an it. This signal was measured from SE lead in EASI electrode configuration (EASI electrode configuration is used in Philips Holter monitoring devices.) in department of automation science and engineering at Tampere University of Technology (TUT). It can be seen how the baseline of the signal is corrected by applying the high-pass filter and also the effect of power-line interference is perfectly removed. On the left side, the whole record is shown and on the right side, zoomed version of the noisy and filtered signals are illustrated for better visualization.

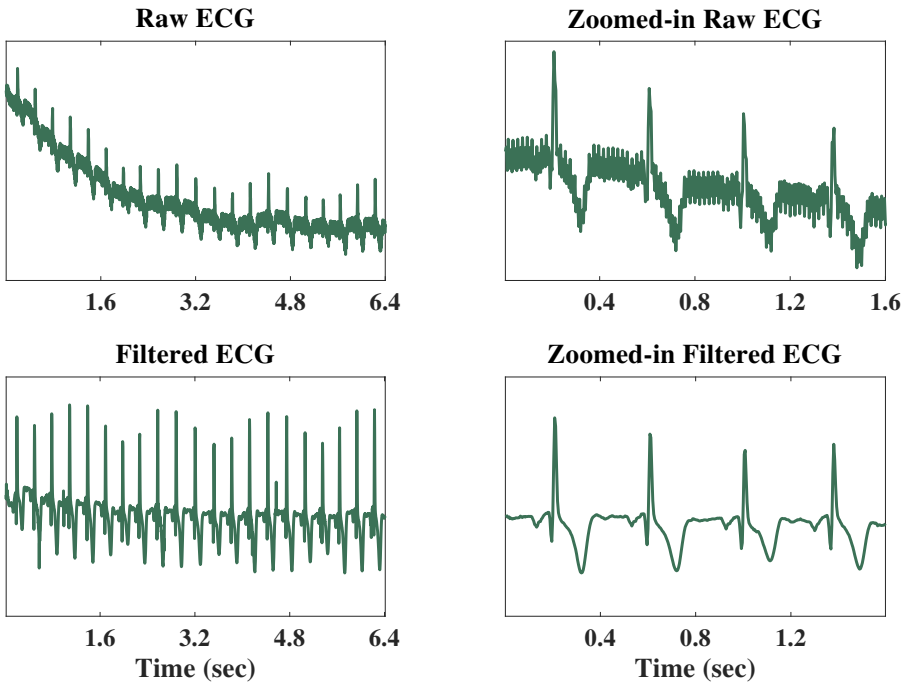

Figure 4.3 *Effect of filtering on a noisy ECG Signal. Top left shows a noisy ECG and top right shows its zoomed version. Bottom rows show the top row record after preprocessing in an original and zoomed version.*

QRS Detection Methods For evaluating three QRS detection methods, each of them individually, was applied on the whole MIT-BIH Arrhythmia database and then the detected R-point were compared to the annotated R-point from annotation file provided in the database.

In Table 4.2, numbers of correctly detected R-peaks (TP), missed R-peaks (FN) and wrongly detected R-peaks (FP) are gathered. According to these scores that were explained in chapter 3.2.3, sensitivity and precision are calculated for each QRS detection method. It can be seen that, the modified Pan-Tompkins method with optimum center frequency and bandwidth for its band-pass filter gave the highest sensitivity and precision. Therefore, result of the modified Pan-Tompkins method was chosen for the further analysis parts. It is worth mentioning that the Area-based R detection method works very well on clean signals but for the corrupted ECG signals and in noisy environments, number of false alarms (or FP) are much higher than the two other methods.

Table 4.2 *Results of three R-peak detection method on MIT-BIH Arrhythmia database.*

	Pan-Tompkins	Modified Pan-Tompkins	Area-based
True Positive (samples)	102123	105381	101736
False Positive (samples)	4220	3877	8912
False Negative (samples)	6519	3261	6906
Sensitivity (%)	94, 00	97, 00	93, 64
Precision (%)	96, 03	96, 45	91, 94

Figure 4.4 shows a short part of ECG signal (from record 114 of MIT-BIH Arrhythmia database) and the results of QRS detection methods on it. It can be observed that all three methods detect R-points very well. Although modified Pan-Tompkins and Area-based methods resulted in more accurate detected fiducial R-points.

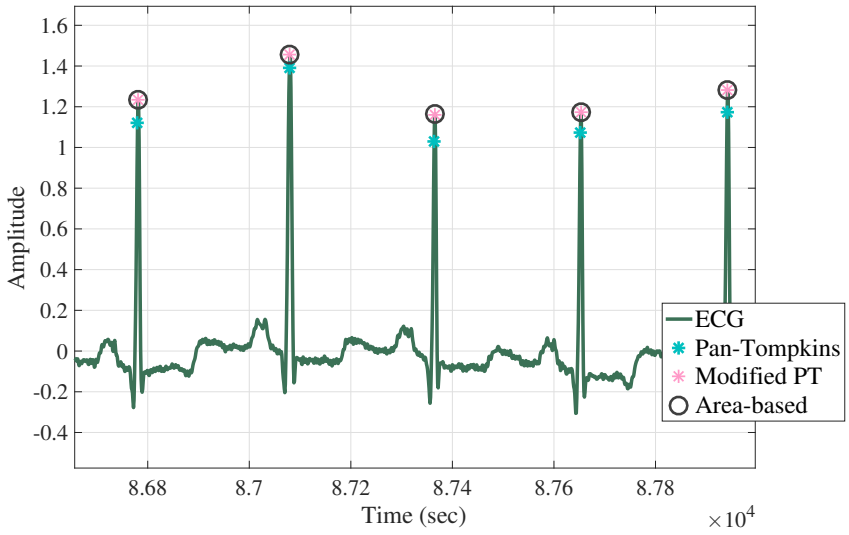

Figure 4.4 *Detected R-points by Pan-Tompkins, modified Pan-Tompkins and Area-based methods are marked with black circle, red star and cyan diamond, respectively for subject 114.*

Ectopic Beats Detection Figure 4.5 illustrates result of the ectopic detection method for record 119 of MIT-BIH Arrhythmia database. As can be seen here and explained in chapter 3.2.4, the principle of ectopic beat detection method was based on RR intervals duration (pink arrows) and amplitude of R-wave peak (light green arrows). There is a clear difference between RR interval duration and R-peak amplitude of ectopic (surrounded by gray ellipse) and normal beats. It is worth mentioning that, although the R-peak detection is not perfect for ectopic beats due to right bundle branch block of subject 119, ectopic detection method perfectly distinguished ectopic beats from normal ones.

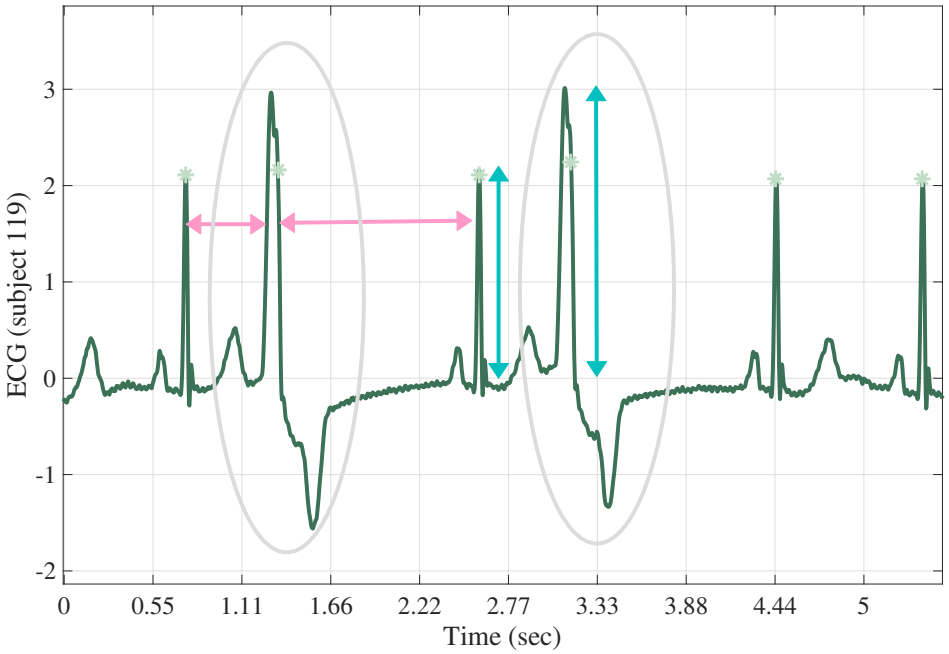

Figure 4.5 *Ectopic beat detection based on RR interval duration and R-peak amplitude for subject 119. Two ectopic beats are highlighted with a gray ellipse around them, it can be seen that the previous RRI is shorter and the next one is longer when ectopic beat happens. In addition, the R-peaks amplitudes are larger in the ectopic beats.*

Table 4.3 presents results of the morphological based ectopic detection method that are compared with the annotations file included in the database. According to the confusion matrix explained in chapter 3.2.9, actual classes correspond to real types of ECG beats based on their annotation file which here positive classes are referred to ectopic/premature beats and negative classes are corresponded to normal beats of ECG signal. The same principle is considered for predicted classes which

are the results of our ectopic detection method. It can be observed that our simple morphological based ectopic beat detection method was able to distinguished ectopic beats from the other beats with $85,74\%$ sensitivity and $84,34\%$ specificity.

Table 4.3 *Confusion matrix of morphological ectopic detection method on MITBIH Arrhythmia database. Actual classes correspond to real types of ECG beats based on their annotation file which here Positive classes are referred to ectopic/premature beats and Negative classed are corresponded to normal/other beats of ECG signal. The same principle is considered for predicted classes which are the results of our ectopic detection method.*

		Actual Classes	
		Positive	Negative
Predicted Classes	Positive	33579	11147
	Negative	5586	60031
		$Sens = 85,74\%$	$Spec = 84,34\%$

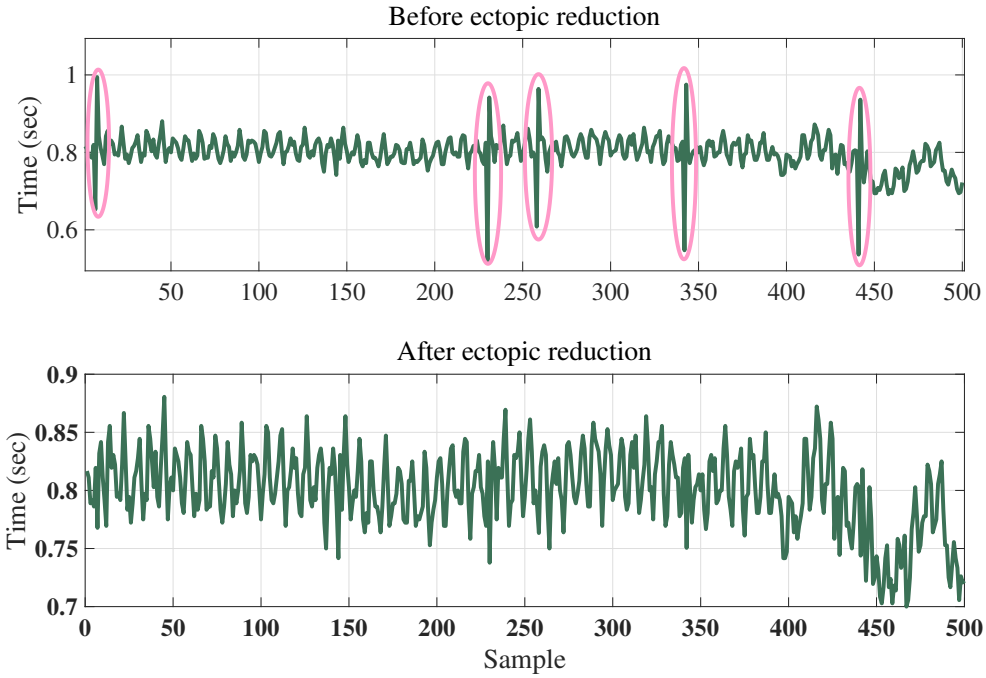

Figure 4.6 *The effect of ectopic reduction on RR intervals from record 110 of MIT-BIH Arrhythmia database. Top: RRI before ectopic beats correction, bottom: RRI after ectopic beats correction*

Ectopic Beats Reduction After detecting the ectopic beats and checking the detected beats with the annotation file, we applied the interpolation of zero degree for reducing the ectopic beats and further heart rate and HRV analysis purposes. Figure 4.6 illustrates an example of RR intervals (obtained from time interval between each two consecutive R-peaks), before and after applying the ectopic reduction method. In the top panel, it can be observed that there are large changes (surrounded by pink ellipses) that represents the occurrence of ectopic beats. It can be seen that how RRI changes are different between normal and ectopic beats. Bottom panel represents the corrected RRI after applying interpolation of zero degree method on the above RRI. It can be seen that the variation of RRI changes is more visible after reducing the ectopic beats.

Heart Rate Analysis Figure 4.7 shows how heart rate has been changed for a subject (record 102 from MIT-BIH Arrhythmia database) during a day. This graph provides a momentary heart rate level (beats/min) to a user and can be used e.g. for monitoring the heart rhythm or controlling the intensity of exercise. Higher values represent time of the day that subject was more active and smaller values show the subject was probably in a more relaxed situation. Green and pink lines show actual heart rate values during the day and the average of heart rate values in every one-hour frame, respectively. The gray arrows indicate different period of the day that heart rate activity of the subject was changed.

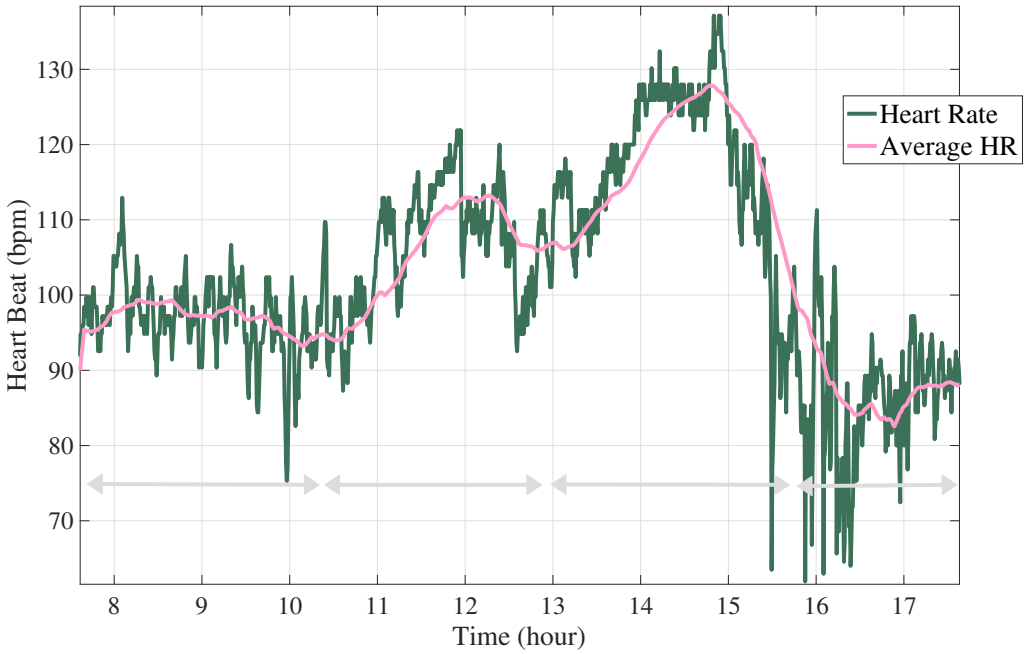

Figure 4.7 *Heart rate changes during a day for record 102*

HRV Parameters In table 4.4 the selected time domain HRV parameters for a 5-minute long frame from subject 102 whose heart rate activity is plotted in Figure 4.7 are presented. These parameters are wildly used in various HRV based algorithms for stress and recovery analysis, metabolic processes and energy expenditure estimation, detection of movements or changes in posture.

Table 4.4 *HRV parameters obtained from a 5-min long ECG frame of record 102*

Subject	SDNN (ms)	RMSSD (ms)	pNN50 (%)	SD1 (ms)	SD2 (ms)
102	38.96	53.07	20	37.59	38.96

PVC Detection algorithms The sum of the trough R-peak with minimum methods were separately applied on the whole MIT-BIH Arrhythmia database. In sum of trough technique, different thresholds and three different ranges for finding the optimal range of n were studied. In Figure 4.8, ROC curve for three different ranges are plotted that are range 11 to 25 (blue curve), range 10 to 60 (pink curve) and

range 35 to 85 (green curve). Each ROC curve represents the changes in threshold values. The threshold values varied from 100 to -100 with steps of 0.01. For each of the ROC curves the area under curve (AUC) is calculated and written on the figure with the same color as its corresponding ROC curve. Based on AUC values for the three studied ranges, it can be concluded that the blue ROC curve that represents the sample range of 11 to 25 after R-peak, gives the largest AUC value of 0.87 in comparison to the other ranges.

Although there is always a tradeoff between higher sensitivity and lower specificity and it highly depends on the application that the algorithm is going to be used in, then if we want to present a threshold for this PVC detection method (sum of trough), threshold of -5 can be chosen. Since it results in highest sensitivity of 87% and specificity of 82% which means the sum of trough PVC detection method with threshold of -5 provides a good detection rate (large number of correctly detected PVC beats) and reasonable number of false alarm.

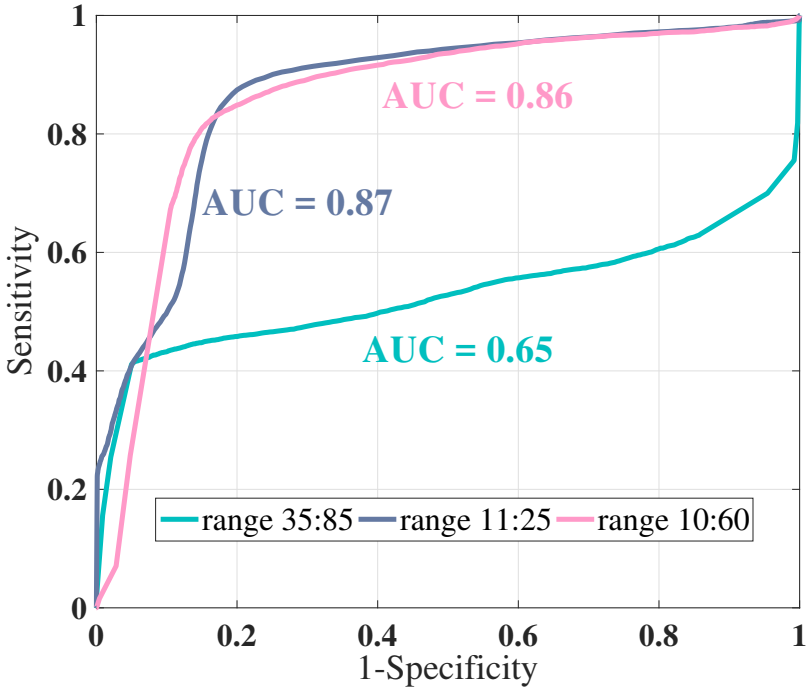

Figure 4.8 *Evaluation of sum of the trough, three ROC curves for three ranges of n (number of samples after R-peaks) are plotted. For each ROC curve the threshold values were varied from -100 to 100 with a step of* 0.01*. The AUC for each curve was also computed and it is written on the figure with the same color as its corresponding ROC curve.*

In Figure 4.9, ROC curve is plotted for discovering the optimum threshold value for the R-peak with minimum method. The threshold value has been changed from -10 to 10 with a step of 0.01. The obtained AUC for this method was 0.75. Here, the same as sum of through method, the best threshold value which resulted in highest sensitivity of 68% and specificity of 72% can be reported at -0.7 for the whole MIT-BIH Arrhythmia database. Therefore, for using these PVC detection methods, optimum values for thresholds and range can be set to the above values that we obtained from the ROC curves.

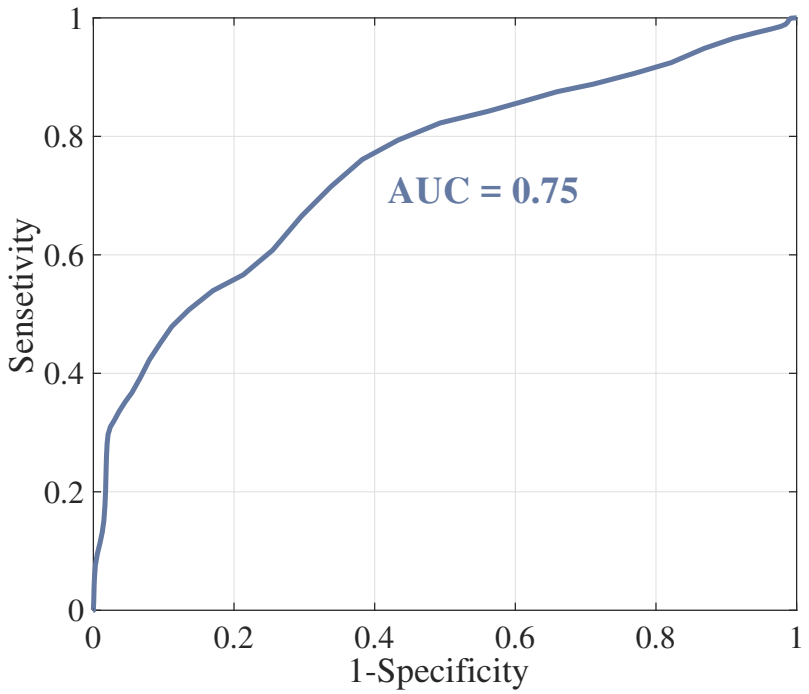

Figure 4.9 *Evaluation of R-peak with minimum: ROC curve is plotted for the threshold values that were varied from -10 to 10 with a step of 0.01. The AUC for this curve is equal to* 0.75.

4.3 IP Analysis

Figure 4.10 shows an IP signal measured from one subject in three phases of standing, walking with 3 km/h, and walking 6 km/h in a continuous measurement. In the first panel, the dashed pink lines show the annotations where the new phases are stabilized. Therefore, probably the measurement phases are changed several seconds before them. There are three small panels that show a magnified version

of three small slices of the signal. It can be seen that the more intense the activity, more the number of cycles (in the 10-second frame) and larger the amplitude of the signals have become. The third panel shows the variation in the respiration rate (calculated by ACF). The large valleys in the respiratory rate are probably due to some deep breaths by the subject. The pink line is a 9th order polynomial fitted to the respiration rate for a better illustration of the increase in this trend.

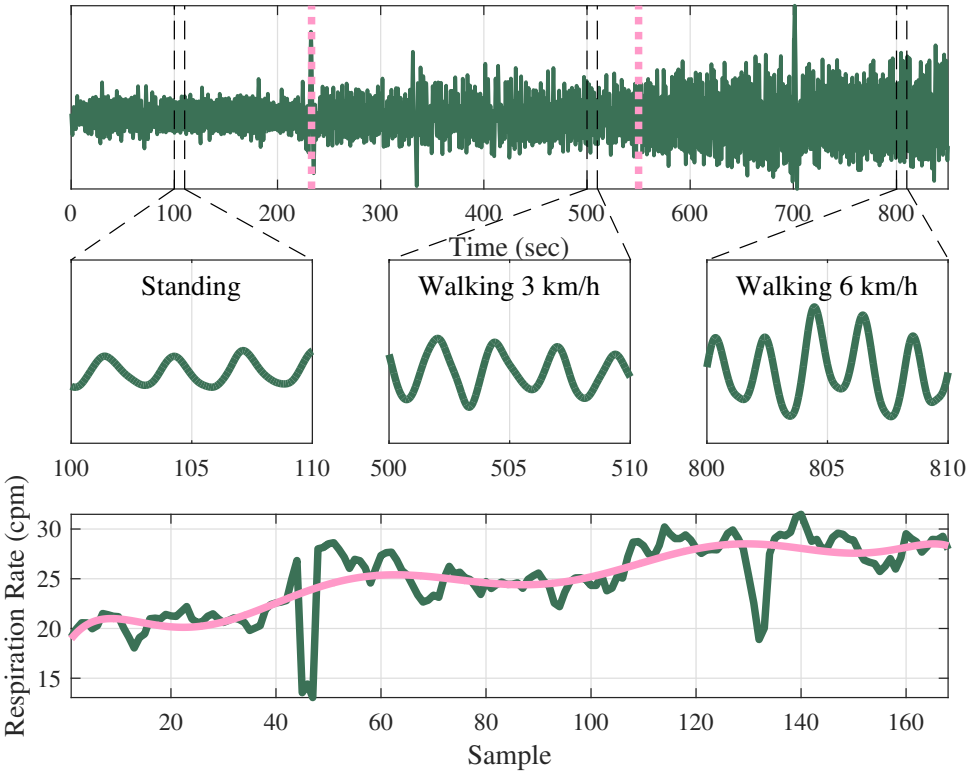

Figure 4.10 *Three magnified slices of IP signal measured in three phases standing, walking with 3 km/h, and walking with 6 km/h, from left to right, respectively. The most bottom panel shows the respiration rate estimated from the signal and a 9-th order polynomial fitted to it.*

The first panel in Figure 4.11 illustrates the temperature signal measured from mask and IP signal measured from subject 2 as an example. It can be seen that the signals follow the same frequency and amplitude changes. Although, it should be noted that this measurement has been done in a steady position and therefore has almost no artefacts. The second panel shows the respiration rate estimated from these two signals. The maximum error in this figure is 0.80 cycles per minute (cpm).

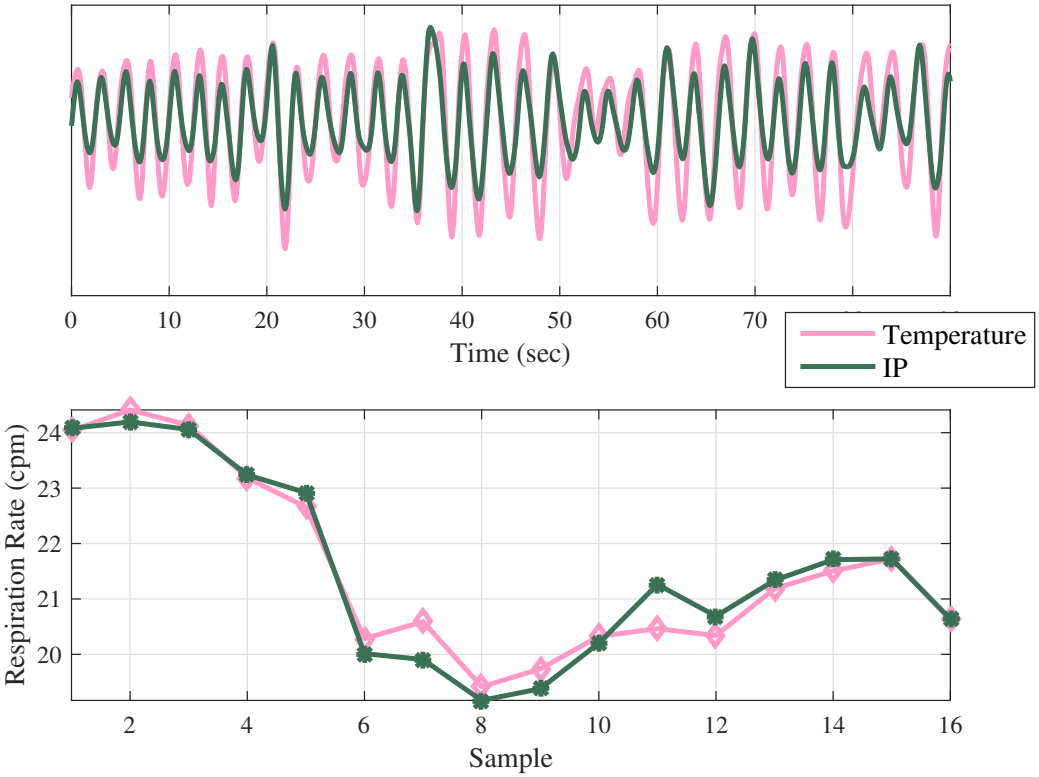

Figure 4.11 *Comparing the IP and temperature mask signals measured from subject 2. The bottom panel shows the respiration rate estimated from these two signals.*

Figure 4.12 shows the correlation between the respiration rate resulted from the IP frames and the ones from the temperature sensor. The pink circles indicate the points in which the error between the two respiration rates were larger than 3 cpm. These points were totally 18 points out of 870 (15 subjects each 58 frames) showing that the error of the 98% of the frames were less than 3 cpm. The dashed blue line shows the regression line fitted to the data. The correlation coefficient is equal to 0.96.

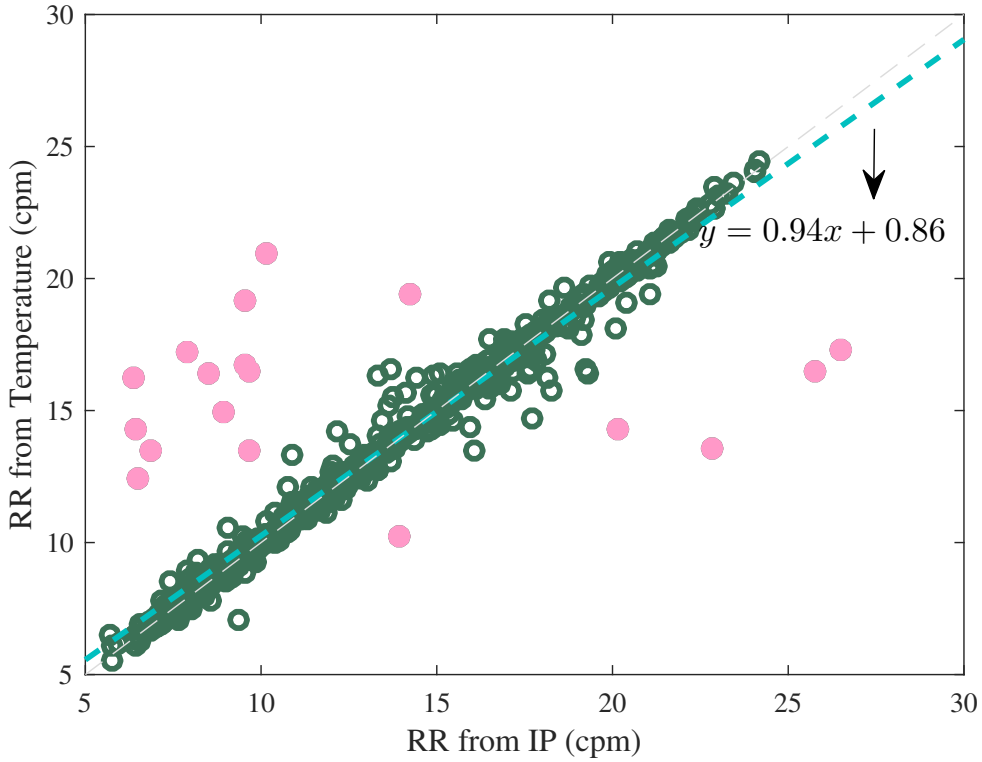

Figure 4.12 *A comparison between the respiration rate estimated from all the frames of the data (from the IP and temperature signals) that are totally 870 frames. The pink circles show the points in which the error is larger than 3 cpm.*

Table 4.5 shows the statistical results of the error. MAE and RMSE are computed between the respiration rate estimated from the IP and the temperature signals. The maximum MAE and RMSE are related to subject 9 and 14, respectively. It is worth pointing out that in Figure 4.12 the 11 points out of 18 pink circles are linked to subjects 9 and 14. The total MAE and RMSE values are 0.40 cpm and 1.20 cpm, respectively. It can be concluded that the respiratory rate estimated from IP signals is quite close to the respiratory rate estimated from temperature masks which is not inconvenient in ambulatory applications. Therefore, the IP signal can be considered as a good alternative for estimating respiratory rate.

Table 4.5 *MAE and RMSE errors between the respiration rate estimated from the IP and the reference temperature signals for all the 15 subjects (10 males and 5 females). The last row shows the total error for all the subjects.*

Subjects	**MAE (cpm)**	**RMSE (cpm)**
1	0.16	0.28
2	0.20	0.29
3	0.15	0.18
4	0.24	0.33
5	0.15	0.20
6	0.33	0.84
7	0.20	0.27
8	0.08	0.11
9	2.06	0.15
10	0.25	0.48
11	0.56	0.26
12	0.15	0.19
13	0.44	1.10
14	0.69	2.06
15	0.34	1.24
average	0.40	1.20

5. CONCLUSIONS AND FUTURE WORKS

In this work, the main goal was towards an automatic digital signal processing approach from physiological signal classification to processing and analyzing the two most vital physiological signals in long-term healthcare monitoring (ECG and IP). In addition, our motivation for designing a generic physiological signal classifier was developing a classification algorithm that can be implemented in automatic healthcare monitoring system with the purpose of merging multiple wearable devices into one piece and simplifying the usage of them for long-term purposes.

The objectives of this master thesis was accomplished very well. A novel generic physiological signal classifier that has the ability to distinguish five types of physiological signals (ECG, Resp, SCG, EMG and PPG) from each other with 100 % accuracy was developed. The novel generic physiological signals classifier proposed in this master thesis work is also published and presented in XIV Mediterranean Conference on Medical and Biological Engineering and Computing 2016 [68]. It should be mentioned that the proposed classifier was not very successful in distinguishing lead I and II of ECG signal from each other (error of 27% was reported) which means that the general purpose features were enough discriminating to recognize different physiological signals from each other but not enough for classifying different ECG leads.

Furthermore, a couple of signal processing methods and algorithms for analyzing ECG and IP signals based on the presented results by their authors was selected and then the selected algorithms were implemented in MATLAB with the aim of long-term physiological signal processing. The analysis approach for ECG signal processing was included these steps: ECG pre-processing, three QRS detection algorithms, ectopic beat detection and reduction technique, heart rate analysis method and PVC detection algorithm. And the implemented approach for IP analysis was included IP pre-processing and respiration rate estimation. In this work, different publicly available databases were used in development and evaluation phases. In

the long run, we have evaluated the implemented signal processing techniques and achieved reasonable performances that were presented in the result chapter.

One part of the future work of this master thesis could be evaluation of the proposed classifier with other databases and also adding other types of physiological signals to the classifier. In addition, the implemented analysis algorithms can be tested with real data measured by e.g. DISSE measurement setup. Although different pre-processing and filtering techniques for eliminating different types of noise, interference and artefacts were included in this work but it is not clear what types of e.g. movement artefact might occur during the wearable measurements and if the implemented techniques can sufficiently remove those artefacts without losing the significant information of the recorded data. In addition to that, since the ultimate goal of DISSE project is to provide a new convenient healthcare system for elderly, methods for detecting other heart arrhythmia such as ST segment elevation or depression can also be studied. Generally, more sufficient signal processing algorithms can be implemented and be tested with real data from elderly patients.

BIBLIOGRAPHY

[1] Gari D Clifford, Francisco Azuaje, and Patrick McSharry. *Advanced methods and tools for ECG data analysis*. Artech House, Inc., 2006.

[2] Tomas B Garcia et al. *12-lead ECG: The art of interpretation*. Jones & Bartlett Publishers, 2013.

[3] Roger Mark. Quantitative physiology: Organ transport systems. *Notes from Principals of Cardiac Electrophysiology Course*, 2000.

[4] Rajarshi Gupta, Madhuchhanda Mitra, and Jitendranath Bera. *ECG acquisition and automated remote processing*. Springer, 2014.

[5] George B Moody and Roger G Mark. The impact of the MIT-BIH arrhythmia database. *Engineering in Medicine and Biology Magazine, IEEE*, 20(3):45–50, 2001.

[6] Kevin G Kinsella and David R Phillips. *Global aging: The challenge of success*, volume 60. Population Reference Bureau Washington, 2005.

[7] Steven C Castle. Clinical relevance of age-related immune dysfunction. *Clinical Infectious Diseases*, 31(2):578–585, 2000.

[8] Arnold Baca, Peter Dabnichki, Mario Heller, and Philipp Kornfeind. Ubiquitous computing in sports: A review and analysis. *Journal of Sports Sciences*, 27(12):1335–1346, 2009.

[9] Yang Hao and Robert Foster. Wireless body sensor networks for health-monitoring applications. *Physiological measurement*, 29(11):R27, 2008.

[10] Robert Istepanian, Swamy Laxminarayan, and Constantinos S Pattichis. *M-health*. Springer, 2006.

[11] Loukianos Gatzoulis and Ilias Iakovidis. Wearable and portable ehealth systems. *IEEE Engineering in Medicine and Biology Magazine*, 26(5):51–56, 2007.

[12] Andreas Lmberis and André Dittmar. Advanced wearable health systems and applications-research and development efforts in the european union. *IEEE Engineering in Medicine and Biology Magazine*, 26(3):29–33, 2007.

[13] Alexandros Pantelopoulos and Nikolaos Bourbakis. A survey on wearable biosensor systems for health monitoring. In *2008 30th Annual International Conference of the IEEE Engineering in Medicine and Biology Society*, pages 4887–4890. IEEE, 2008.

[14] Alexandros Pantelopoulos and Nikolaos G Bourbakis. A survey on wearable sensor-based systems for health monitoring and prognosis. *IEEE Transactions on Systems, Man, and Cybernetics, Part C (Applications and Reviews)*, 40(1):1–12, 2010.

[15] Louis Atallah, Benny Lo, and Guang-Zhong Yang. Can pervasive sensing address current challenges in global healthcare? *Journal of Epidemiology and Global Health*, 2(1):1–13, 2012.

[16] Lei Clifton, David A Clifton, Marco AF Pimentel, Peter J Watkinson, and Lionel Tarassenko. Gaussian processes for personalized e-health monitoring with wearable sensors. *Biomedical Engineering, IEEE Transactions on*, 60(1):193–197, 2013.

[17] Jaakko Malmivuo and Robert Plonsey. *Bioelectromagnetism: principles and applications of bioelectric and biomagnetic fields*. Oxford University Press, USA, 1995.

[18] Arnold M Katz. *Physiology of the Heart*. Lippincott Williams & Wilkins, 2010.

[19] Gerard J Tortora and Bryan H Derrickson. *Principles of anatomy and physiology*. John Wiley & Sons, 2008.

[20] Carey R Merritt, H Troy Nagle, and Edward Grant. Fabric-based active electrode design and fabrication for health monitoring clothing. *Information Technology in Biomedicine, IEEE Transactions on*, 13(2):274–280, 2009.

[21] Subhasis Chaudhuri, Tanmay D Pawar, and Siddhartha Duttagupta. *Ambulation analysis in wearable ECG*. Springer Publishing Company, Incorporated, 2009.

[22] Adam Gacek and Witold Pedrycz. *ECG signal processing, classification and interpretation: a comprehensive framework of computational intelligence*. Springer Science & Business Media, 2011.

[23] Philip De Chazal, Maria O'Dwyer, and Richard B Reilly. Automatic classification of heartbeats using ECG morphology and heartbeat interval features. *IEEE Transactions on Biomedical Engineering*, 51(7):1196–1206, 2004.

[24] Bert-Uwe Kohler, Carsten Hennig, and Reinhold Orglmeister. The principles of software QRS detection. *IEEE Engineering in Medicine and Biology Magazine*, 21(1):42–57, 2002.

[25] Natalia M Arzeno, Zhi-De Deng, and Chi-Sang Poon. Analysis of first-derivative based qrs detection algorithms. *IEEE Transactions on Biomedical Engineering*, 55(2):478–484, 2008.

[26] Masahiko Okada. A digital filter for the qrs complex detection. *IEEE Transactions on Biomedical Engineering*, 12(26):700–703, 1979.

[27] Valtino X Afonso, Willis J Tompkins, Truong Q Nguyen, and Shen Luo. ECG beat detection using filter banks. *IEEE Transactions on Biomedical Engineering*, 46(2):192–202, 1999.

[28] Jiapu Pan and Willis J Tompkins. A real-time QRS detection algorithm. *Biomedical Engineering, IEEE Transactions on*, (3):230–236, 1985.

[29] Patrick S Hamilton and Willis J Tompkins. Quantitative investigation of QRS detection rules using the MIT-BIH arrhythmia database. *IEEE Transactions on Biomedical Engineering*, (12):1157–1165, 1986.

[30] Qiuzhen Xue, Yu Hen Hu, and Willis J Tompkins. Neural-network-based adaptive matched filtering for QRS detection. *IEEE Transactions on Biomedical Engineering*, 39(4):317–329, 1992.

[31] Berdakh Abibullaev and Hee Don Seo. A new QRS detection method using wavelets and artificial neural networks. *Journal of Medical Systems*, 35(4):683–691, 2011.

[32] Riccardo Poli, Stefano Cagnoni, and Guido Valli. Genetic design of optimum linear and nonlinear QRS detectors. *IEEE Transactions on Biomedical Engineering*, 42(11):1137–1141, 1995.

[33] Gao Zhengzhong, Kong Fanxue, and Zhang Xu. Accurate and rapid QRS detection for intelligent ECG monitor. In *2011 Third International Conference on Measuring Technology and Mechatronics Automation*, volume 1, pages 298–301. IEEE, 2011.

[34] Juan Arteaga-Falconi, Hussein Al Osman, and Abdulmotaleb El Saddik. R-peak detection algorithm based on differentiation. In *Intelligent Signal Processing (WISP), 2015 IEEE 9th International Symposium on*, pages 1–4. IEEE, 2015.

[35] Galen S Wagner. *Marriott's practical electrocardiography*. Lippincott Williams & Wilkins, 2001.

[36] Ik-Sung Cho and Hyeog-Soong Kwon. PVC classification algorithm through efficient R wave detection. *Journal of Sensor Science and Technology*, 22(5):338–345, 2013.

[37] Supat Ittatirut, Apiwat Lek-uthai, and Arporn Teeramongkonrasmee. Detection of premature ventricular contraction for real-time applications. In *Electrical Engineering/Electronics, Computer, Telecommunications and Information Technology (ECTI-CON), 2013 10th International Conference on*, pages 1–5. IEEE, 2013.

[38] A García, H Romano, E Laciar, and R Correa. Development of an algorithm for heartbeats detection and classification in holter records based on temporal and morphological features. In *Journal of Physics: Conference Series*, volume 332, page 012023. IOP Publishing, 2011.

[39] Robert Chen-Hao Chang, Chih-Hung Lin, Ming-Fan Wei, Kuang-Hao Lin, and Shiue-Ru Chen. High-precision real-time premature ventricular contraction (PVC) detection system based on wavelet transform. *Journal of Signal Processing Systems*, 77(3):289–296, 2014.

[40] Abbas K Abbas, Konrad Heimann, Katrin Jergus, Thorsten Orlikowsky, and Steffen Leonhardt. Neonatal non-contact respiratory monitoring based on real-time infrared thermography. *Biomedical Engineering Online*, 10(1):1, 2011.

[41] Nicole Verginis, Margot J Davey, and Rosemary SC Horne. Scoring respiratory events in paediatric patients: Evaluation of nasal pressure and thermistor recordings separately and in combination. *Sleep Medicine*, 11(4):400–405, 2010.

[42] John M Shneerson. *Sleep medicine: a guide to sleep and its disorders*. John Wiley & Sons, 2009.

[43] Jerome J Freundlich and James C Erickson. Electrical impedance pneumography for simple nonrestrictive continuous monitoring of respiratory rate, rhythm and tidal volume for surgical patients. *Chest Journal*, 65(2):181–184, 1974.

[44] SL Hill, JP Blackburn, and TR Williams. Measurement of respiratory flow by inductance pneumography. *Medical and Biological Engineering and Computing*, 20(4):517–518, 1982.

[45] Leila Mirmohamadsadeghi and Jean-Marc Vesin. Respiratory rate estimation from the ECG using an instantaneous frequency tracking algorithm. *Biomedical Signal Processing and Control*, 14:66–72, 2014.

[46] Paul A Leonard, J Graham Douglas, Neil R Grubb, David Clifton, Paul S Addison, and James N Watson. A fully automated algorithm for the determination of respiratory rate from the photoplethysmogram. *Journal of Clinical Monitoring and Computing*, 20(1):33–36, 2006.

[47] David Prutchi and Michael Norris. *Design and development of medical electronic instrumentation: a practical perspective of the design, construction, and test of medical devices*. John Wiley & Sons, 2005.

[48] Development and clinical application of impedance pneumography technique, 2014. Available: `http://dspace.cc.tut.fi/dpub/handle/123456789/22669`.

[49] Kundan Nepal, Eric Biegeleisen, and Taikang Ning. Apnea detection and respiration rate estimation through parametric modelling. In *Bioengineering Conference, 2002. Proceedings of the IEEE 28th Annual Northeast*, pages 277–278. IEEE, 2002.

[50] Alistair EW Johnson, Sharath R Cholleti, Timothy G Buchman, and Gari D Clifford. Improved respiration rate estimation using a kalman filter and wavelet cross-coherence. In *Computing in Cardiology 2013*, pages 791–794. IEEE, 2013.

[51] Walter Karlen, Srinivas Raman, J Mark Ansermino, and Guy A Dumont. Multiparameter respiratory rate estimation from the photoplethysmogram. *IEEE Transactions on Biomedical Engineering*, 60(7):1946–1953, 2013.

[52] Shin-Shin Chuang, Kung-Tai Wu, Chen-Yang Lin, Steven Lee, Gau-Yang Chen, and Cheng-Deng Kuo. Poincaré plot analysis of autocorrelation function of RR intervals in patients with acute myocardial infarction. *Journal of Clinical Monitoring and Computing*, 28(4):387–401, 2014.

[53] Bram Lohman, Olga Boric-Lubecke, VM Lubecke, PW Ong, and MM Sondhi. A digital signal processor for doppler radar sensing of vital signs. *IEEE Engineering in Medicine and Biology Magazine*, 21(5):161–164, 2002.

[54] Guanghao Sun and Takemi Matsui. Rapid and stable measurement of respiratory rate from doppler radar signals using time domain autocorrelation model. In *2015 37th Annual International Conference of the IEEE Engineering in Medicine and Biology Society (EMBC)*, pages 5985–5988. IEEE, 2015.

[55] Seismocardiography: Practicalimplementation and feasibility, 2014. Available: `http://urn.fi/URN:ISBN:978-952-60-5875-7`.

[56] Carlo J De Luca. The use of surface electromyography in biomechanics. *Journal of Applied Biomechanics*, 13:135–163, 1997.

[57] John Allen. Photoplethysmography and its application in clinical physiological measurement. *Physiological Measurement*, 28(3), 2007.

[58] MA Garcia-Gonzalez, A Argelagós, Mireya Fernández-Chimeno, and J Ramos-Castro. Differences in QRS locations due to ECG lead: relationship with breathing. In *XIII Mediterranean Conference on Medical and Biological Engineering and Computing 2013*, pages 962–964. Springer, 2014.

[59] Examples of Electromyograms at http://www. physionet.org [online]. available: https://physionet.org/physiobank/database/emgdb/. [accessed: 01- oct- 2015].

[60] Mikko Peltokangas, Antti Vehkaoja, Jarmo Verho, Matti Huotari, Juha Roning, and Jukka Lekkala. Monitoring arterial pulse waves with synchronous body sensor network. *Biomedical and Health Informatics, IEEE Journal of*, 18(6):1781–1787, 2014.

[61] Han-Wook Lee, Ju-Won Lee, Won-Geun Jung, , and Gun-Ki Lee. The periodic moving average filter for removing motion artifacts from PPG signals. *International Journal of Control Automation and Systems*, 5(6):701, 2007.

[62] Angkoon Phinyomark, Chusak Limsakul, Huosheng Hu, Pornchai Phukpattaranont, and Sirinee Thongpanja. *The usefulness of mean and median frequencies in electromyography analysis*. INTECH Open Access Publisher, 2012.

[63] T Eftestøl, SO Aase, and JH Husøy. Spectral characterization of ECG in out-of-hospital cardiac arrest patients. In *Computers in Cardiology, 1999*, pages 707–710. IEEE, 1999.

[64] Susana Blanco, Arturo Garay, and Diego Coulombie. Comparison of frequency bands using spectral entropy for epileptic seizure prediction. *ISRN Neurology*, 2013.

[65] U Rajendra Acharya, H Fujita, Vidya K Sudarshan, Shreya Bhat, and Joel EW Koh. Application of entropies for automated diagnosis of epilepsy using EEG signals: A review. *Knowledge-Based Systems*, 88:85–96, 2015.

[66] Riccardo Bellazzi and Blaz Zupan. Predictive data mining in clinical medicine: current issues and guidelines. *International Journal of Medical Informatics*, 77(2):81–97, 2008.

[67] Mukta Paliwal and Usha A Kumar. Neural networks and statistical techniques: A review of applications. *Expert systems with applications*, 36(1):2–17, 2009.

[68] Shadi Mahdiani, Jukka Vanhala, and Jari Viik. A novel generic algorithm for robust physiological signal classification. In *XIV Mediterranean Conference on Medical and Biological Engineering and Computing 2016*, pages 1038–1043. Springer, 2016.

[69] James C Huhta and John G Webster. 60-Hz interference in electrocardiography. *Biomedical Engineering, IEEE Transactions on*, (2):91–101, 1973.

[70] Soo-Chang Pei and Chien-Cheng Tseng. IIR multiple notch filter design based on allpass filter. *Circuits and Systems II: Analog and Digital Signal Processing, IEEE Transactions on*, 44(2):133–136, 1997.

[71] Shadi Mahdiani, Vala Jeyhani, and Antti Vehkaoja. A review of transient suppression methods of IIR notch filters used for power-line interference rejection in ECG measurement. In *XIV Mediterranean Conference on Medical and Biological Engineering and Computing 2016*, pages 151–156. Springer, 2016.

[72] SooChang Pei and Chien-Cheng Tseng. Elimination of AC interference in electrocardiogram using IIR notch filter with transient suppression. *Biomedical Engineering, IEEE Transactions on*, 42(11):1128–1132, 1995.

[73] J Piskorowski. Powerline interference removal from ECG signal using notch filter with non-zero initial conditions. In *Medical Measurements and Applications Proceedings (MeMeA), 2012 IEEE International Symposium*, pages 1–3, 2012.

[74] JA Van Alste and TS Schilder. Removal of base-line wander and power-line interference from the ECG by an efficient FIR filter with a reduced number of taps. *IEEE Transactions on Biomedical Engineering*, (12):1052–1060, 1985.

[75] Fernando Soares Schlindwein, AC Yi, Tim Edwards, and ICH Bien. Optimal frequency and bandwidth for FIR bandpass filter for QRS detection. In *Advances in Medical, Signal and Information Processing, 2006. MEDSIP 2006. IET 3rd International Conference On*, pages 1–4. IET, 2006.

[76] Yangdong Liao, Ru-Xin Na, and Derek Rayside. Accurate ECG R-peak detection for telemedicine. In *Humanitarian Technology Conference-(IHTC), 2014 IEEE Canada International*, pages 1–5. IEEE, 2014.

[77] Rangaraja M Rangayyan and Narender P Reddy. Biomedical signal analysis: a case-study approach. *Annals of Biomedical Engineering*, 30(7):983–983, 2002.

[78] Barbara Mali, Sara Zulj, Ratko Magjarevic, Damijan Miklavcic, and Tomaz Jarm. Matlab-based tool for ECG and HRV analysis. *Biomedical Signal Processing and Control*, 10:108–116, 2014.

[79] Task Force of the European Society of Cardiology et al. Heart rate variability standards of measurement, physiological interpretation, and clinical use. *European Heart Journal*, 17:354–381, 1996.

[80] Mika P Tarvainen, J-P Niskanen, JA Lipponen, PO Ranta-Aho, and PA Karjalainen. Kubios HRV, a software for advanced heart rate variability analysis. In *4th European Conference of the International Federation for Medical and Biological Engineering*, pages 1022–1025. Springer, 2009.

[81] Vala Jeyhani, Tiina Vuorinen, Matti Mäntysalo, and Antti Vehkaoja. Comparison of simple algorithms for estimating respiration rate from electrical impedance pneumography signals in wearable devices. *Health and Technology*, pages 1–11.